FORMAT FOR THE APPROVAL PAGE

To: Dr. Saundra F. Delauder, Dean of Graduate Studies and Research

The members of the Committee approved the Thesis of YURY MARKUSHIN
Student's Name
as presented on 09/24/2013.
Date

We recommend that it be accepted in partial fulfillment of the requirements for the degree of Master of Applied Optics with a major in Optics.

Department Physics & Eng Date 09/30/2013
Advisor

Department PHYSICS & ENGINEERING Date 09/30/13
Member

Gour chyam Pati Department Physics and Engineering Date 09/30/2013
Member

Affiliation Mathematical Sci Date 09/30/2013
Outside Member

APPROVED

Department Physics & Eng. Date 09/30/2013
Program Director

College CMNST Date 10/04/13
Dean

Date 10/07/13
Dean, School of Graduate Studies and Research

A DIRECT-DETECTION SCANNING LADAR

WITH THREE-DIMENSIONAL IMAGING CAPABILITY:

SYSTEM DEVELOPMENT AND PERFORMANCE ANALYSIS

by

YURY Y. MARKUSHIN

A THESIS

Submitted in partial fulfillment of the requirements
for the Master's degree in Applied Optics
in the Optics Graduate
Program of Delaware State University

DOVER, DELAWARE

2013

Acknowledgements

Foremost, I would like to thank my advisors Dr. R. Tripathi and Dr. G. S. Pati for being patient and supportive with theoretical and experimental difficulties related to this project. Their guidance helped me enormously throughout the research, building LADAR prototype from scratch and writing this thesis. Without their invaluable help the current work would not be possible. I would like to recognize Nicholas P. Calvano who has been a very dedicated worker in our lab and spend a lot of time and effort on LabView programming and polarimeter design which will be implemented in the next generation LADAR system. I would also like to thank the team members of our research laboratories "*Photonic Imaging & Information Processing Laboratory*" and "*Atom Photonics Laboratory*": Alexey Chibisov, Zach Warren, David Riser and Michael Williams for their everyday help, research enthusiasm, project related suggestions and ideas. I would like to thank Mr. Nick Quigley for his help designing and building many of the mechanical components in the DSU machine shop. I would like to recognize Dr. Poopalasingam Sivakumar for his help with LabView programming and code optimization. I would like to thank my family for giving me birth, believing in me and supporting both financially and spiritually throughout my college career. I'm extremely grateful to my wonderful fiancée Yongjing for being understanding and supportive in my endeavors. I also want to acknowledge other members of my thesis committee: Prof. Lott from the Department of Mathematical Sciences, and Prof. Khan from the Department of Physics & Engineering. Last, but not least, I would like to thank Delaware State University, and the Optical Sciences Center for Applied Research (OSCAR) in the Department of Physics & Engineering for helping me with a two year fellowship.

The instrumentation necessary to conduct our research was made possible from the financial support from NSF MRI grant # 1039675 and NASA URC-5 grant # NNX09AU90A.

A DIRECT-DETECTION SCANNING LADAR

WITH THREE-DIMENSIONAL IMAGING CAPABILITY:

SYSTEM DEVELOPMENT AND PERFORMANCE ANALYSIS

by

YURY Y. MARKUSHIN

A THESIS

Submitted in partial fulfillment of the requirements

for the Master's degree in Applied Optics

in the Optics Graduate

Program of Delaware State University

DOVER, DELAWARE

2013

Acknowledgements

Foremost, I would like to thank my advisors Dr. R. Tripathi and Dr. G. S. Pati for being patient and supportive with theoretical and experimental difficulties related to this project. Their guidance helped me enormously throughout the research, building LADAR prototype from scratch and writing this thesis. Without their invaluable help the current work would not be possible. I would like to recognize Nicholas P. Calvano who has been a very dedicated worker in our lab and spend a lot of time and effort on LabView programming and polarimeter design which will be implemented in the next generation LADAR system. I would also like to thank the team members of our research laboratories "*Photonic Imaging & Information Processing Laboratory*" and "*Atom Photonics Laboratory*": Alexey Chibisov, Zach Warren, David Riser and Michael Williams for their everyday help, research enthusiasm, project related suggestions and ideas. I would like to thank Mr. Nick Quigley for his help designing and building many of the mechanical components in the DSU machine shop. I would like to recognize Dr. Poopalasingam Sivakumar for his help with LabView programming and code optimization. I would like to thank my family for giving me birth, believing in me and supporting both financially and spiritually throughout my college career. I'm extremely grateful to my wonderful fiancée Yongjing for being understanding and supportive in my endeavors. I also want to acknowledge other members of my thesis committee: Prof. Lott from the Department of Mathematical Sciences, and Prof. Khan from the Department of Physics & Engineering. Last, but not least, I would like to thank Delaware State University, and the Optical Sciences Center for Applied Research (OSCAR) in the Department of Physics & Engineering for helping me with a two year fellowship.

The instrumentation necessary to conduct our research was made possible from the financial support from NSF MRI grant # 1039675 and NASA URC-5 grant # NNX09AU90A.

Abstract

Laser Detection and Ranging (LADAR) is an established optical sensing technology for creating three-dimensional image of the target object using the time-of-flight (TOF) and intensity information. LADAR technology has applications in areas such as agriculture, archeology, geology, meteorology, astronomy, robotics, military and law enforcement. For instance, LADAR systems are used to obtain terrain maps during planetary exploration missions or detecting enemy tanks hidden under camouflaged nets.

A basic direct detection scanning LADAR system consists of two main parts: a transmitter and a receiver. Transmitter arm employs a Q-switched Nd:YAG pulsed laser operating at 1064 nm and a fast-scanning two-axis galvanometric mirror steering system. The receiver arm employs a large aperture telescope, focusing optics and a sensitive linear mode APD with a fast (500 ps, in our case) rise time. The system scans the target in pixel-by-pixel manner and collects the fraction of scattered/back-reflected light using the telescope. Intensity of back-reflected light is measured using the APD and the TOF is measured using a *Time-to-Amplitude* converter (TAC). Both intensity and range images are plotted simultaneously which provides an explicit three-dimensional (3D) information about the object.

In this thesis, I will discuss the design, performance metrics, and operation of the direct detection scan-LADAR system and present the results obtained. The depth resolution of the system is decided by the duration of the pulse. Our setup yields approximately 15 cm of depth resolution. The spatial resolution is directly related to the divergence of the laser pulse. The current system has a beam divergence angle of about 3 mrad, yielding approximately 30 cm beam spot at 100 m propagation distance. With the speed constraint imposed by electronics, 50×50 pixels image can be obtained in about 25 seconds. High resolution 90×90 pixels image takes 90 seconds to acquire.

The future development of the system will include incorporating an in-line polarimeter into the scan-LADAR system. The polarimetric scan-LADAR will have the ability to see parts of the scene not visible under intensity-only-imaging, such as objects hidden behind highly reflective surfaces.

Table of Contents

List of Figures

Chapter 1: Introduction to LADAR

LADAR (Laser Detection and Ranging) technology is an established optical sensing tool with wide applications in areas such as aviation, agriculture, archaeology, geology, meteorology, astronomy, robotics, military and law enforcement. In agriculture, a LADAR system can be used to create a topographic map of the farmer's land to reveal the slopes and the areas with an optimal sun exposure for growing crops [1]. These measurements can help farmers to utilize the land more efficiently and to save on expensive fertilizers. In archeology, a LADAR system can provide researchers with an ability to obtain high resolution digital elevation models of the archeological site, exposing micro topography previously hidden by vegetation, etc [2]. LADAR technology has the ability to penetrate through forest canopy which can lead to discovery of features not visible otherwise. Range information measured by a LADAR system corresponds to the features hidden under the flat vegetated surfaces such as fields. LADAR technology is also widely used in geology [3]. High resolution digital elevation maps of Earth surface were created using airborne LADARs which lead to discoveries related to origin and evolution of our planet and enables researchers to conduct studies on concurrent physical and chemical processes in the Earth's core [4]. Combination of LADAR technology with General Positioning System (GPS) allows creating extremely accurate terrain maps used for aviation, soil survey and landscape analyzes [5,6].

The LADAR technology has applications in meteorology and environmental studies [7]. It is used to study atmospheric composition and structure of clouds and aerosols. Differential Absorption LADAR (DIAL) is used for range based measurements of greenhouse gases in the atmosphere [8].

Doppler LADARs are used to measure the temperature and vertical wind profiles [9]. In astronomy, LADAR systems are used to determine position of the moon with millimeter precision, which is needed to conduct general relativity experiments [10]. In robotics, the LADAR technology is used for general perception of the environment and classification of surrounding objects and targets [11]. As a LADAR system can create precise 3-D topographic maps of a terrain and yield precise range information for the same, this technology can be used for safe landing and obstacles avoidance for manned and unmanned vehicles. LADARs are also used for obstacle avoidance and target identification for fully autonomous robotic planes. NASA is using LADAR systems to obtain surface maps of the landing sites during planetary exploration missions [12]. High resolution of airborne or ground based LADAR systems can capture enough details to identify targets such as tanks, in conditions when other imaging techniques cannot be used. This makes LADAR technology very attractive for military applications, mainly as a high precision imaging identification tool. Remote sensing LADARs are also used for detection of chemical and biological warfare agents in the atmosphere [13]. In law enforcement, a LADAR speed gun is used by the police for speed limit enforcement purposes [14].

LADAR is an active, remote sensing technique that is similar to RADAR (Radio Detection and Ranging) but uses laser pulses instead of the radio waves.

It works on the principle of transmitting and receiving the electromagnetic energy, typically in the wavelength range of 1 to 11 microns.

A LADAR can detect a reflecting target in the area of interest as well as the distance to the target (range), by measuring the intensity and the time delay of short duration pulses sent by the transmitter [15]. Amplitude of the received return pulse carries information about reflective properties of the target.

Radial velocity and direction of a moving target can also be measured by detecting a Doppler frequency shift produced by a moving target. It is equal to the difference in frequencies between the transmitted and received signals. A typical LADAR system has two major parts: a transmitter, and a receiver. The transmitter consists of the laser light source and transmitting optics. The receiver consists of the collection optics and a photo-detector. Laser generated pulse of light launched towards the target by using a telescope or a system of lenses. Once the light pulse hits the target, it reflects and/or scatters depending on the reflective and diffusive properties of the material. Part of the back-reflected/scattered light is collected by the collection optics, and routed to a sensitive photo-detector. The detector transforms the captured light energy into the electric signal which is processed to obtain the required information about the target [16]. The photocurrent generated by the detector is directly proportional to the intensity of incident light. There are two main configurations of a LADAR system: bi-static and mono-static (fig.1.1). In the bi-static configuration the receiving and the transmitting arms have separate paths. In the mono-static configuration a single arm is used to launch the light pulse towards the target and to receive the return pulse. The advantage of a mono-static configuration is its compactness.

The advantage of a bi-static configuration is elimination of coupling of noise produced by the transmitted beam into receiving channel of a LADAR system.

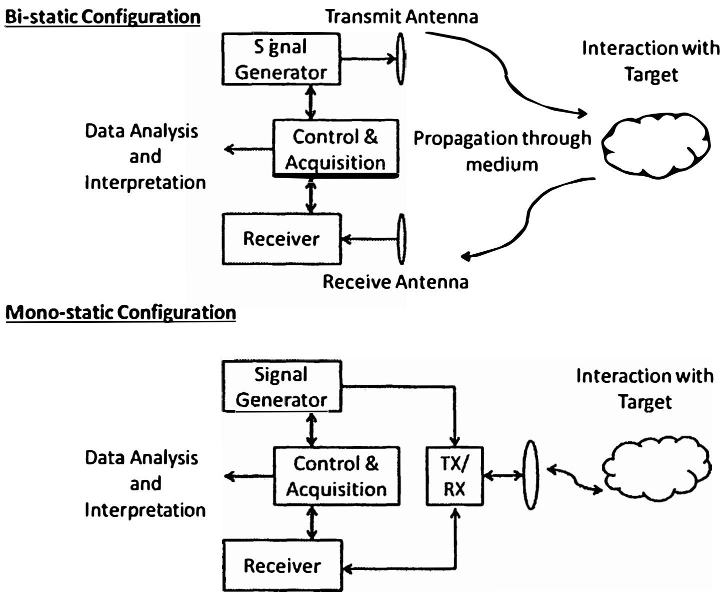

Figure 1.1. Schematic of bi-static and mono-static LADAR configuration

1.1. Characteristics of LADAR System

Electromagnetic energy travels with the speed of light ‘c’ in vacuum. A relationship between the distance to the target (called range R) and the time it takes for the light to travel from the transmitter to the target and come back to the receiver (called roundtrip time t) is given by the following expression:

$$t = \frac{2R}{c} \tag{1.1}$$

By definition, the range resolution of a LADAR system is defined as the smallest longitudinal separation between two objects that could be detected by the LADAR.

In fig.1.2, a LADAR system illuminates a structure made with two surfaces a and b, separated by a distance ΔR [17].

In the first case (a) the spot size of the beam is small and each surface is individually illuminated with a respective single pulse. Separation between the two surfaces ΔR can be defined as

$$\Delta R = R_1 - R_2 \tag{1.2}$$

where R_1 and R_2 are range measurements made by LADAR for surfaces a and b respectively.

In the second case (b) the spot size of the illuminating beam is large and both surfaces are illuminated simultaneously with a single pulse.

We can relate Time-of-Flight (TOF) to the range as:

$$\mathrm{t} + \tau = \frac{2(\mathrm{R} + \Delta \mathrm{R})}{\mathrm{c}} \tag{1.3}$$

here τ is the TOF corresponding to the distance between surface a and surface b. The LADAR system should be able to resolve the separation ΔR so that the corresponding TOF τ could be detected. We can subtract the two equations and obtain time of flight for ΔR:

$$t - t + \tau = \frac{2R}{c} + \frac{2\Delta R}{c} - \frac{2R}{c} \Rightarrow \tau = \frac{2\Delta R}{c} \tag{1.4}$$

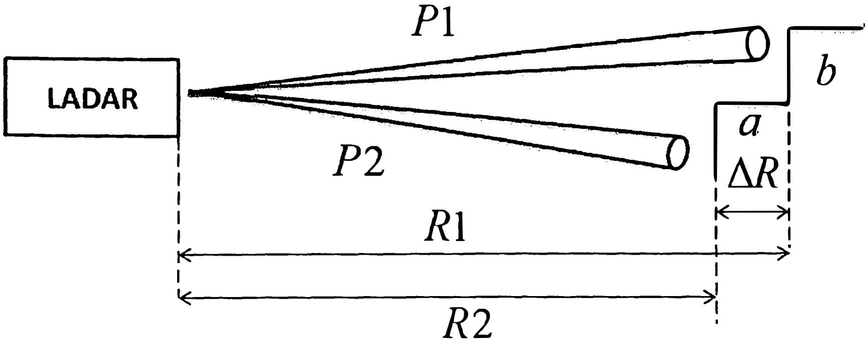

(a) Objects illuminated separately with individual pulses

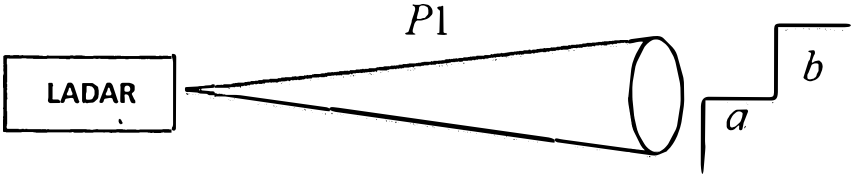

(b) Objects illuminated simultaneously with a single pulse

Figure 1.2. Resolution of LADAR system

In practice, the duration of the pulse ultimately decides how small of a τ the LADAR system can measure. Another important characteristic of the LADAR system is the divergence angle of the illuminating beam. As the laser beam propagates towards the target, the physical size of the beam increases due to diffraction. The angular divergence (or angular beamwidth) of the beam can be described by the following expression:

$$\theta_t = \frac{1.22\lambda}{D_t} \tag{1.5}$$

where D_t is the diameter of the aperture of the transmitting optics. For a scanning-LADAR system, the systems usually have beamwidth much smaller than the size of the target.

Using this model we can calculate the intensity of light reaching the detector's aperture via free space propagation:

$$I_{t\arg et} = \frac{4P_t}{\pi(\theta_t R)^2} \tag{1.7}$$

where P_t is transmitted power and θ_t is angular divergence of the beam defined in eqn. 1.5. Small angle approximation was used for this calculation and propagation losses were not taken into account. When light travels through the atmosphere, some amount of energy is also lost in absorption/scattering by molecules and dust particles. The average value of atmospheric absorption can be represented as:

$$A = e^{-(a+b)R} \tag{1.8}$$

where a is absorption coefficient due to absorption by atmospheric gas molecules and b is scattering coefficient due to Rayleigh scattering from dust particles.

We can rewrite the intensity on the target equation by including the atmospheric loss:

$$I_{t\arg et} = \frac{4AP_t}{\pi(\theta_t R)^2} \tag{1.9}$$

This expression assumes the ability of the target to completely reflect the laser light. It is not true for most real-world materials. Typical reflectivity (ρ_t) values for a target may vary from 2 % to 25 % under normal conditions. Highly polished metallic surfaces and white snow can reflect as much as 80 %. Another important parameter deciding the amount of light return to the receiver is the surface area of the target.

In order to compute it, we need to first determine the relationship between the LADAR receiver's field-of-view (FOV) and the angular size of the target.

We can assume the target to be of square shape for simplicity. The FOV of the receiver can be determined from the angular size target approximated as the length of square's side divided by the distance of the receiver from the target. The light collected by the receiver is focused into the photo-detector with a square aperture. We can find the instantaneous field of view (IFOV) γ of the receiver by dividing the size of a square detector (D_R) by the effective focal length of an optical system (f_l) which focuses light into the detector i.e. -

$$\gamma = \frac{D_R}{f_l} \tag{1.10}$$

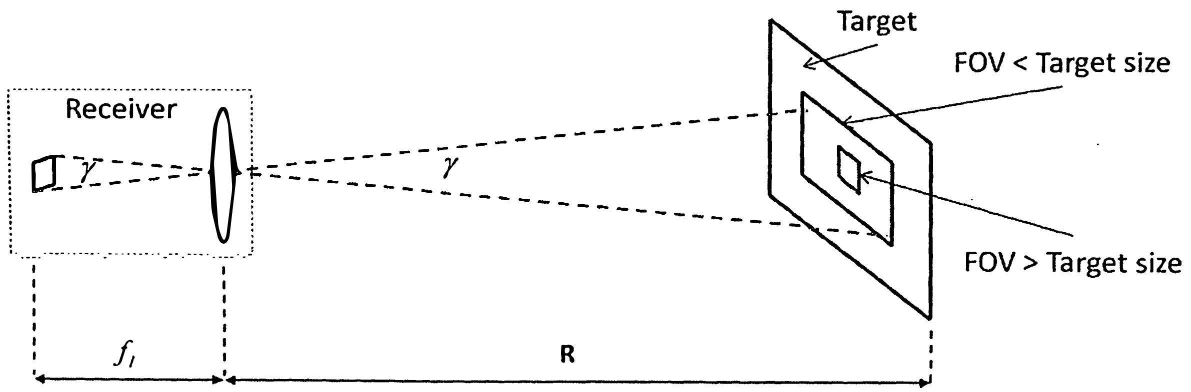

Figure 1.4. FOV of LADAR System

In a case when the illuminating laser beam is smaller than FOV and angular size of the target (refer to Fig 1.4. above), the effective area of the target (dA) is equal to the projected area of the beam at the target:

$$dA = \frac{\pi \theta_t^2 R^2}{4} \tag{1.11}$$

If FOV of the receiver is smaller than the angular size of the target (refer to Fig 1.4. above) then the effective surface area is calculated using the following expression:

$$dA = (\gamma \times R)^2 \tag{1.12}$$

We can compute the amount of power reflected from the target by multiplying the intensity of light at the target by reflectivity and effective surface area of the target:

$$P_{reflected} = I_{t\arg et} \times \rho_t \times dA = \frac{4AP_t}{\pi(\theta_t R)^2} \times \rho_t \times dA \tag{1.13}$$

1.3. Scattering of Reflected Light from the Target

The laser light can reflect from the target in many different ways depending on the material characteristics of the target. For mirror-like targets, there is a specular reflection of light where the incoming light reflects in a single outgoing direction in such a way that reflected angle is equal to the incident angle. In this case, the angular divergence of the outgoing beam from the target remains unchanged.

Optically rough surfaces (i.e. Lambertian targets) disperse laser light in all directions (Fig. 1.5.) so that the angular beamwidth of the outgoing beam is much larger than that of the incoming one. The laser light gets dispersed over a solid angle θ_R which equals to π steradians for Lambertian targets and equals to the transmitted angular beam diameter squared θ_t^2 steradians for specular targets [19].

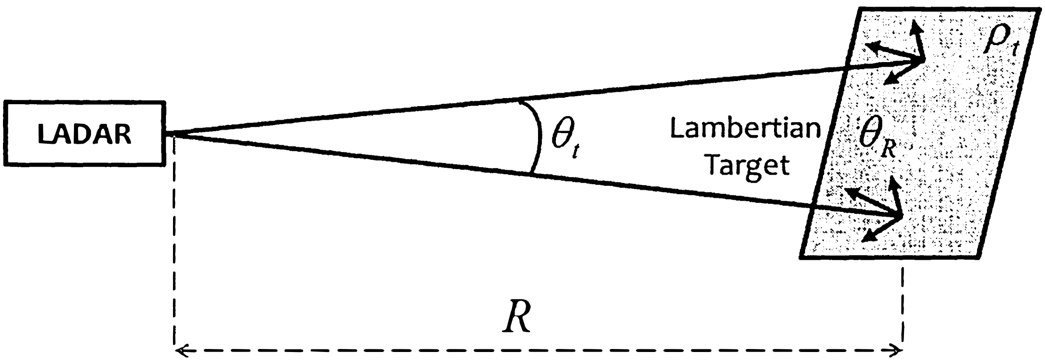

Figure 1.5. Lambertian target scattering of light

For surfaces that are not entirely specular or Lambertian the values between θ_t^2 and π are possible. In this simplified model we assume that the laser beam is incident normal to the target surface and the reflected light enroute LADAR receiver is spread over the surface area outlined by the spherical section of the solid angle. We calculate the intensity of the light entering the receiver:

$$I_{receiver} = \frac{P_{reflected}}{R^2 \theta_R} A \tag{1.14}$$

By assuming that the receiver has a circular aperture of diameter D_R, we can calculate the power received by multiplying this intensity by the area of receiver aperture:

$$P_{receiver} = \frac{A\pi D_R^2 P_{reflected}}{4R^2\theta_R} \tag{1.15}$$

The above equation shows that optical power $P_{receiver}$ received at the receiver varies as $1/R^2$ which is equivalent to the dependence on R in a one-way communication system. One can use this relation to determine the maximum range distance R_{max} for the LADAR by knowing the threshold detection power level at the receiver.

Note that while maximum range distance R_{max} is decided by the power in the transmitted optical pulse, the range resolution of LADAR defined in eqn. (1.4) is decided by the duration of the optical pulse.

1.4. Receiver Efficiency

The efficiency of a LADAR system is defined as the ratio of transmitted and received signals. It is composed of two components: optical transmission of receiver optics and quantum efficiency of the detector. First component, the transmission of optics, determines the fraction of light arriving at the photo-detector which is calculated from the total amount of light arriving at the receiver. By taking the transmissivity of components (T) into account we can write the equation showing the power seen by the detector:

$$P_{\det} = \frac{TA^2 D_R^2 \rho_t (dA) P_t}{R^2 \theta_R (\theta_t R)^2} \tag{1.16}$$

The number of photo-electrons produced by the light incident on the detector is equal to the corresponding power multiplied by the integration time of the detector, divided by photon energy. We can write an equation that describes a fraction of light incident on the detector that is converted into an electrical signal [20]:

$$i_{sig} = \eta \overline{N} = \eta \frac{P_{\det} \Delta t}{h\nu} = \eta \left(\frac{T A^2 D_R^2 \rho_t (dA) P_t}{R^2 \theta_R (\theta_t R)^2 h\nu} \right) \Delta t \tag{1.17}$$

where η is a quantum efficiency of the detector, $\overline{N}$ is the average number of photons incident on the detector's aperture, Δt is an integration time of the detector, h is Planck's constant, and ν is the frequency of incident light.

1.5. Sources of Noise in LADAR System

There are many sources of noise in a typical LADAR system. Typically, these originate from the statistical fluctuations of the light incident on the photo-detector, noise introduced by the system, and the unwanted light. The most fundamental source of noise in the LADAR system is the photon counting noise. The number of photo-electrons registered by the detector during the integration time is a random variable proportional to the expected number of photons. Since photons arrive at the detector at random times, there is an uncertainty in the number of photons measured during the finite time window. In the presence of noise, the photocurrent can be written as $i(t) = i_{sig} + i_N(t)$.

If the noise current i_N represents a stationary random process with Poisson statistics (white noise), the photocurrent variance due to photon counting noise can be calculated from:

$$\sigma_{pc}^2 = \langle i_N^2 \rangle = 2 q_e B \, i_{sig} \tag{1.18}$$

where q_e is electronic charge, and B is the detector bandwidth. The variance of photon counting (or shot) noise also gives the rms noise power. Therefore, the shot noise limited signal-to-noise ratio (SNR) for the LADAR system is given by:

$$SNR = \frac{Avg.\ signal\ power}{Noise\ power} = \frac{i_{sig}^2}{\sigma_{pc}^2} = \frac{i_{sig}}{2 q_e B} \tag{1.19}$$

Note that the shot noise limited SNR increases with i_{sig} which is proportional to the power received at the detector. Depending on the system, other sources of noise may dominate over the shot noise and impose a limit on the maximum detectable range, R_{max} for the LADAR.

The second source of noise (in a coherent LADAR system) is the laser speckle noise. It is caused by the interference from a large number of independent coherent radiators which occurs when the coherent laser reflects from the target surface.

Variance of photocurrent due to speckle noise can be calculated using the following equation:

$$\sigma_{sp}^2 = E[N_{signal}]\left(1 + \frac{N_{signal}}{M}\right) \tag{1.20}$$

where $E[N_{signal}]$ is the average number of photoelectrons produced by the detector, M is a number of degrees of freedom of light (M = 1 for fully coherent light, M $\rightarrow \infty$ for fully incoherent light).

The third source of noise (dominant in a photon-counting LADAR system) is from thermal noise. Since any object which is above absolute zero temperature causes random motion of electrons, the photon-detector used in the system itself generates noise. Thermal noise present in a LADAR system can be evaluated from the dark current count of the detector. Dark current is defined as the current produced by the detector in absence of any external photons.

Finally, fourth major source of noise in a LADAR system originates from the background noise caused by any extraneous light collected by the detector. The examples of the background noise can be sunlight or ambient light collected by the detector that contains no information about the target.

Chapter 2: Types of LADAR Systems

LADAR systems can be divided into three main categories: 1. pulsed LADAR (scanning LADAR, flash LADAR), 2. photon counting LADAR and 3. coherent LADAR. A summary of these systems is shown in fig. 2.1.

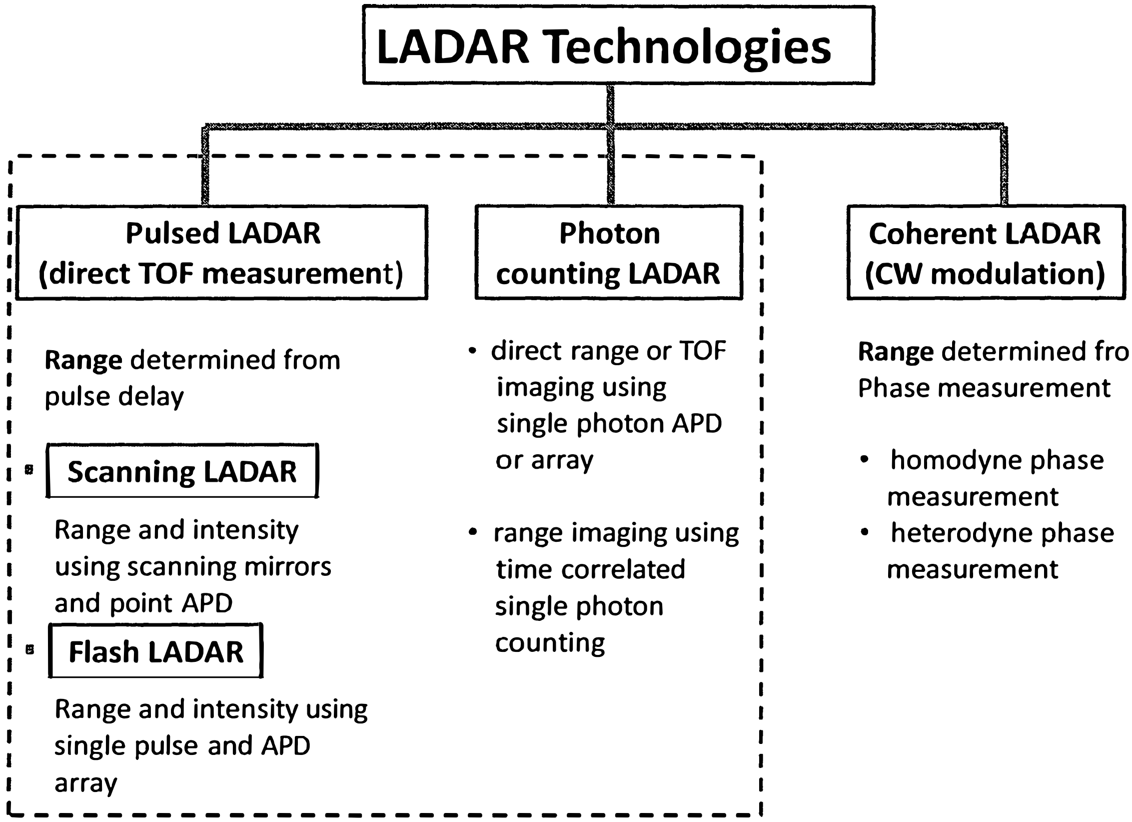

Figure 2.1. Overview of LADAR system technologies

2.1. Pulsed LADAR Systems

The simplest direct detection TOF LADAR system is based on a short pulse laser, receiving optics and a timing circuit. A laser pulse illuminates the target and the reflected light is captured by the receiving optics. The travel time-of-flight of the pulse is measured by the timing circuit.

2.1a Scanning LADAR

A scanning LADAR system scans the target point-by-point with a laser beam by using scanning mirrors, and collects the reflected/scattered light from the target to recreate an image of the target. The scanning LADAR is designed with three main components: laser source, scanner and detector. The laser source, with typical wavelength range of 600-1550 nm, is used to illuminate the target. The laser beam scans the target point-by-point by using an x-y scanner [21]. Rate at which the images are developed is greatly affected by the scanner speed. A single avalanche photo-detector (APD) is typically used as a point detector to capture the intensity information of sequential individual pixels. Additional hardware, such as Time-of-Flight Multiscaler (MCA) or Time-to-Amplitude Converter (TAC), is required for data processing and for range information calculation. Three dimensional images of a target can be formed by superposition of intensity and range information.

2.1b Flash LADAR

Instead of mechanically scanning the target using a scanner, a flash LADAR illuminates the scene simultaneously with a single shot of diffused laser light and uses a focal plane array (FPA) as the detector [22]. The FPA has rows and columns of detector pixels. Each pixel has an independent trigger and counter to record the time-of-flight of the laser pulse. Compared to a scanning LADAR system, the flash LADAR system requires a high energy pulsed laser for its operation. On the other hand, the flash LADAR can operate at a much faster rate compared to the scanning LADAR as no mechanical scanning is involved.

Focal Plain Array is a 2 dimensional chip composed of multiple, individually addressable photo-detectors [23]. In order to use the FPAs for range measurements in a LADAR system an appropriate timing electronics must be added for each individual detector. If the focal array size is not big enough to cover the entire field-of-view, the system needs to be scanned in a similar manner as in scanning LADAR. The main difference between FPA and the scanning LADAR is that the first one relies on the number of independent range measurements equal to the number of pixels in the focal array, while scanning LADAR obtains a single range data point for each pixel of the target. The range measurements in case of FPA LADAR must be made in parallel. The main requirement for that is simultaneous illumination of each pixel in the detector array using a single focusing lens. That leads to a dramatic increase in required laser power: n × n focal plane array would mean n^2 increase in power [24].

There are also a few alternative solutions to increased power of the laser which include increasing an aperture of collecting optics, using of fiber light amplifiers or employing a single-photon sensitive detector [25].

2.1.1. Limitations of Pulsed (Direct Detection) LADAR

Imperfect optics and atmospheric dispersion causes the laser pulse beam shape to expand with range. For example, if the laser has a beam divergence of, say, 4 mrad, the beam spot at a distance of 100 m would be about 40 cm. Beam divergence contributes to the fundamental experimental error of the direct detection LADAR technology. If the range is sufficiently high (10-15 km) the beam will have a conical shape due to the divergence in the atmosphere. In this case, photons of a single pulse hitting different targets will arrive at the detector at different times. A single pixel of a LADAR image frame will have more than one valid light return. Ideally, the LADAR system should have a single intensity value for each pixel of the scene. However, with multiple returns not a single value but an array of values is collected for each pixel since any strong return above the noise floor is treated as a valid signal. These values are averaged and reported as a single range per pixel. As a result of the averaging non-existent phantom points are introduced into the point cloud. Also, detection in a pulsed time-of-flight LADAR is limited in resolution by the bandwidth of the detector as well as by the bandwidth of the digitizer used for data capture. Detector with a bandwidth of 10 GHz and a digitizer that can reach 4 GS/s sampling rate yield the following direct detection resolution limit:

$$t = \frac{1}{S} = \frac{1}{4 \times 10^9 \, S/s} = 250 \, ps \tag{2.1}$$

Therefore, the range resolution is limited to the 250 ps roundtrip, which corresponds to 125 ps one way trip or 75 mm minimum range distance. The pulse width of the illuminating laser also affects the range resolution.

Digitizers work best with sharp rise time pulses. In order to overcome the fundamental resolution limit, 'super resolution' algorithms can be used. These methods are based on combining information from multiple low resolution images to create a single high resolution image.

2.2. Photon Counting LADAR

Photon counting LADAR uses a Geiger mode photon detector in the receiving arm, instead of direct detection system's linear mode APD [26]. It operates on the principle called time-correlated single photon counting (TCSPC). TCSPC is based on the detection of single photons of light, recording the detection times and reconstructing the signal using the individual time measurements. When the photon is detected, the arrival time of the corresponding detector pulse is recorded into the register. After many photons are detected the distribution of signal detection builds up producing a distribution of photon probability [27]. The light intensity is represented by the density of the pulses, not by its amplitude as in the case of linear mode APD. The photon counting LADAR has an advantage of imaging long range targets compared to the linear mode direct detection LADAR.

2.3. Coherent LADAR: Continuous Wave (CW) Modulation

An unmodulated continuous wave laser cannot be used for range measurements in coherent LADAR. In order to measure the range, transmitted laser beam needs to be modulated separately from the local oscillator. In the following section, we describe two amplitude modulation techniques that are used in coherent LADAR detection for improving the accuracy in range resolution measurement.

2.3a Amplitude Modulation Technique

In this method, the light is modulated at a single sinusoidal frequency f. Phase shift between transmitted and received signals can be calculated using equation below:

$$\Delta\phi = 2\pi f t_{RT} = 2\pi \left(\frac{2R}{c}\right) \tag{2.2}$$

where t_{RT} is a roundtrip time and R is a distance to the target, which can be calculated from the phase difference and frequency as:

$$R = \frac{c\Delta\phi}{4\pi f} \tag{2.3}$$

The range resolution in this amplitude modulation technique is inversely proportional to the light modulation frequency. Accuracy in range measurement is directly proportional to signal-to-noise ratio (SNR) in the phase measurement. Increasing the modulation frequency will also yield higher accuracy. However, the maximum allowed (i.e., measurable) range reduces with increasing f. This causes aliasing and false target detection if the target is located farther from the maximum allowed range.

One of the solutions to this problem could be using multiple frequencies (chirp modulation) in a single system. The lower frequency can be used for longer range measurements while the higher frequencies can be used for higher accuracy. We will describe it next.

2.3b Chirped Amplitude Modulation

Using a chirped amplitude modulation, it is possible to obtain multiple range readings from each pixel of a target. Chirp is a pulse in which the frequency is linearly changing with time.

Chirp modulation LADAR systems usually have a start chirp frequency of 200 MHz and a stop frequency 800 MHz. The range resolution (ΔR) for this system is given by the following expression:

$$\Delta R = \frac{c}{2\Delta F} \tag{2.6}$$

where ΔF is difference between the start and stop frequencies [28]. The main limitation of the chirped amplitude modulation LADAR is the complicated chirp generating hardware that adds size, noise and cost to the system.

2.3.1. Coherent LADAR

In a coherent LADAR system, the return signal is optically mixed with the reference signal. A highly stable continuous wave laser is usually used as reference signal (local oscillator). Two wavefront matched signals are combined together using a heterodyne mixer and focused on a photo-detector as shown on fig.2.2.

A local oscillator utilized to mode-lock the laser and also to illuminate the heterodyne mixer simultaneously This method is used to produce a response limited only by a shot noise and not sensitive to background light [29].

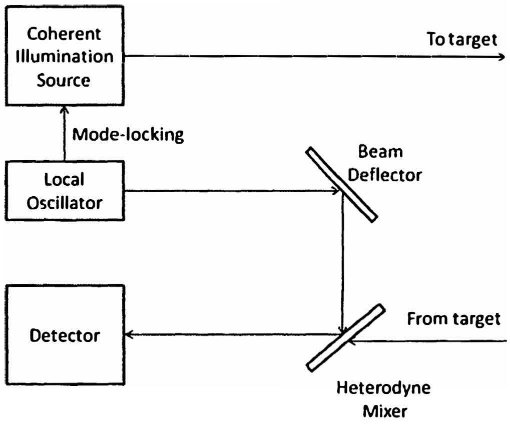

Figure 2.2. Coherent LADAR schematic

The intensity on the detector can be calculated using following model:

$$I(t) = c\varepsilon_0[E_{LO}^2 + E_S + 2E_{LO}E_S\cos((\omega_S - \omega_{LO})t)] \tag{2.7}$$

where E_{LO} is the local oscillator electric field amplitude, E_S is a received signal electric field amplitude, ω_S is a received signal electric field frequency, ω_{LO} is local oscillator signal electric field frequency. The power on the detector can be calculated the following way:

$$P_{\text{det}} = P_{LO} + P_S + 2\sqrt{\gamma P_{LO} P_S}\cos(2\pi\Delta f t + \theta) \tag{2.8}$$

where $P_{LO} = \int c\varepsilon_0 |E_{LO}|^2 dA$, $P_S = \int c\varepsilon_0 |E_S|^2 dA$, $2\pi\Delta f t = \omega_S - \omega_{LO}$, θ is the phase difference between E_{LO} and E_S, γ is heterodyne mixing efficiency. This mathematical expression consists of three components: the power on the detector from the local oscillator, the power from the return signal reflected or scattered from the target and the interference power. In this system amplification occurs in the optical domain, making system immune to thermal noise. This feature makes a coherent LADAR system more accurate than a direct detection one [30].

With coherent detection technique it is possible to obtain a very high range resolution and accuracy within the specific range band. Since the range information is contained in the interference term, the frequency shift between transmitted and received signal indicates range information. A small frequency difference between these signals would correspond to a short range and a large frequency difference would correspond to a long range. A coherent LADAR system requires use of high precision optics.

In order to generate the interference signal, the reflected signal and local oscillator signal must be spatially and temporally coherent, perfectly aligned, and must have the same polarization state to generate interference at a frequency equal to their frequency difference. Accuracy of a coherent LADAR system depends on three main parameters: chirp bandwidth, return light signal-to-noise ratio and the number of samples acquired.

Chapter 3: LADAR Beam Steering Technology

A scanning LADAR system requires scanning of the target pixel-by-pixel in order to illuminate the target with the laser beam and then collect reflected light to obtain range and intensity information. In this chapter, we will describe some of the technologies currently available to perform high speed beam steering (or scanning) for LADAR.

3.1. Galvanometric Mirror Scanner

A two axis galvanometric scanner consists of two reflecting mirrors necessary to create a two- dimensional scan of the target, and two electric motors that drive the mirrors. One of the mirrors in galvo-scanner is typically responsible for x-positioning of the laser beam. Second mirror is responsible for y-positioning of the beam. While working together, the mirrors can steer the beam to scan a specified surface. The main limiting factor of this technology is the speed at which the electric motors can rotate the mirrors. Currently the resonant frequency of the high performance galvanometric motors used in LADAR systems limited to about 3 KHz [31].

3.2. Polygonal Scanner

Polygonal scanner overcomes the main limiting factor of the galvanometric mirror scanners, namely slow scanning speed. Modern polygonal scanners used in LADAR systems yield scanning speeds of 30 KHz. High speed scanning is the main advantage of this type of scanner. A single asymmetric polygon with 16-plane mirror facets can be used to achieve the beam scanning by simply rotating the mirror using a high speed AC synchronous motor [32]. Scanning speeds up to 60 frames per second can be achieved using a 3600 rpm motor.

The main disadvantage of the polygonal mirror scanning technology is complex optical design of the component, limitation of the step size by the number of polygon planes as well as the cross-scan and bowtie errors caused by wobble of the mirror and imperfect alignment.

3.3. Scanning Micro Mirrors Array

Scanning Micro Mirrors are made using semiconductor manufacturing technology and also known as Micro-Electro-Mechanical-Systems (MEMS). Modern MEMS have millions of micro-mirrors on a single chip that can deflect with frequencies of up to 66 KHz [33]. These mirrors require very small power to operate. The range of rotation for these micro-mirrors is typically limited to about 6 degrees. Scanning micro mirrors can be used in LADAR systems since it creates a large number of micro beams that can scan the target from different angles and positions allowing better resolution and accuracy than traditional beam steering techniques [34]. The disadvantage of this technology is that they suffer from cross-scan errors and reduced longevity.

3.4. Acousto Optic Scanners

Acousto-optic scanners employ the sound waves propagating in optical materials to control the refractive index of the material and therefore the angle of an output beam.

A typical two-dimensional acousto-optic based scanner has two beam deflectors that achieve an angular deflection range of up to 10 degrees and scanning frequency of a few KHz. An acousto-optic device acts as a grating, diffracting the laser beam when it passes through. The angular deflection is proportional to the frequency of the sound wave. The main problem associated with this technology is the large absorption of the acousto-optic material which is about 80 % depending on wavelength [35].

3.5. Electro Optic Scanners

Electro-optic devices work by varying the properties of optical materials by application of voltages. An altering input voltage can cause the variation in polarization state of light which affects the degree to which the beam deflects through the material [36]. The deflection range for electro-optic scanners is typically limited to less than 2 degrees.

3.6. Holographic Scanners

Holography is an optical information storage process where the amplitude and phase of light illuminating the recording medium makes permanent changes to the medium, creating a three-dimensional image. A hologram can act as a traditional refracting lens. When the laser beam comes in contact with such a hologram, the beam is getting deflected and focused [37]. A transition of the hologram in respect to the beam will result in scanning angular motion of the output beam. This kind of motion can be generated by the xy-micro translation stage. As in case of polygonal scanners, holographic scanners suffer from bowtie and wobble-type errors.

Chapter 4: Components for Scanning LADAR System Development: Concepts and Strategies

In this chapter, we provide a description of the working principles of some of the major components and devices used in developing a scanning LADAR system. First, we will discuss the components and devices used for performing beam scanning operation in our system.

4.1. Beam Scanning using Galvanometric System

A galvanometric system, GVS002, is used for beam scanning. The GVS002 is a dual axis mirror positioning system with two mirrors and motor assemblies, mounting bracket, two driver cards and two heat sinks [38]. The mirrors in GVS002 have protective silver coating designated for longer wavelengths (i.e. near-infrared). A galvanometer has a high precision motor with a travel range, usually no more than 25 degrees, and acceleration directly proportional to the current applied to the motor. When current is applied to the motor, the shaft completes an arc-like motion. If reverse polarity current is applied the motor immediately comes to stop. If current is turned off, the motor shaft stops due to friction on the shaft. Galvanometer has two main components: the motor that moves the mirror and the detector that works as a feedback circuit providing positioning information to the system. The motor is based on a moving magnet. The magnet is incorporated into the rotor (moving part of the motor) and the coil is a part of the stator (stationary part of the motor). Mirror positioning detector consists of four photodiodes and a light source.

As the position of the mirror changes, the photodiodes detect different amounts of light producing the current correlated with the position of the rotor.

The mirror is attached to the end of the rotor and reflects the light beam over the angular range of the motor. The servo driver circuit translates the currents from the mirror positioning detector to the actual position of the rotor. Then it outputs currents onto the motor to shift the mirror to the user specified position. The galvanometric scanner accepts analog voltage input scaled from -10 to 10 V. The full range amplitude provides a mechanical movement range from -12.5 to 12.5 degrees.

The galvanometric mirror positioning system is aligned using an optical system in such a way that a laser beam hits the x-axis mirror at 90 degree angle as shown in fig.4.1. The scanning range can be calculated by using the following expression:

$$L = 2d \times \tan\alpha \tag{3.2}$$

where d is the distance to the screen, α is the angular range. For example, if we assume d = 10 m and α = 12.5 degrees the scanning range L = 4.4 m.

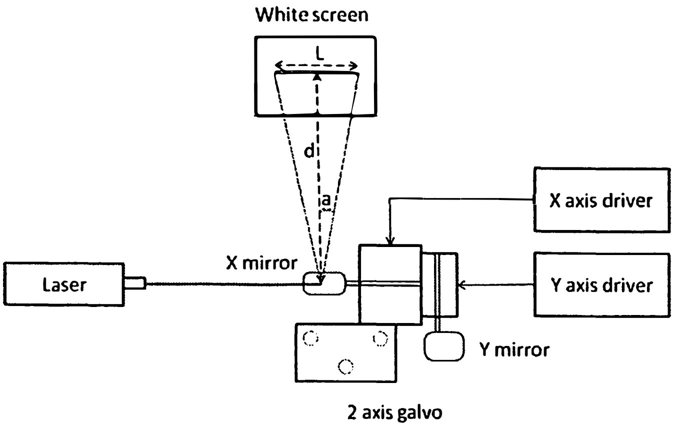

Figure 4.1. Scanning Galvanometric Mirror System for Beam Scanning

4.2 Start and Stop Detectors

A scan-LADAR system built in our laboratory uses two linear mode APDs as the start and stop detectors. The start detector is used to trigger the data acquisition hardware (will be described further in section 4 chapter 5) and for TOF measurements. The stop detector is used to collect intensity of light reflected/scattered from the target and also for TOF measurements.

4.2.1 Start Detector: Linear Mode Avalanche Photo Detector (APD)

An avalanche photodiode is a semiconductor device which employs a photoelectric effect to convert incident photons into an electric current. Linear mode APDs generate an electric signal with an amplitude linearly dependent on the intensity of incident light at the detector's aperture. Linear mode APDs are typically operated at high reverse bias voltage (10-300V), slightly below breakdown region for a specific material used. In this configuration carriers are excited by absorbed photons, accelerated in the presence of a strong electric field generating secondary carriers (i.e. photo-multiplication).

The avalanche process allows generating multiple electrons in response to each incident photon providing a significant amplification to the photocurrent permitting detection of very low light levels. An advantage of high avalanche amplification is that less electronic amplification is needed than with standard PN detectors, reducing the detector's susceptibility to electronic noise and also decreasing the response time of a device, which in other case may be limited by the external amplifier. On the other hand, the avalanche process is a subject to quantum noise and internal amplification noise.

Due to the quantum nature of avalanche process, APD generates excess noise which also gets amplified. Amplification factor and responsivity of the APD strongly depend on the applied reverse bias voltage.

For the LADAR system there are 3 main requirements for the APD:

1. Operating wavelength of the laser needs to be sufficiently close to the APD's central wavelength maximizing the quantum efficiency of the detector.
2. Response time of the detector should be sufficiently fast so that the APD can react on individual pulses coming at a high rate
3. Sensitivity of the APD should be sufficient so that it can detect very low light returns.

4.2.2 Stop Detector: Near Infrared Avalanche, Thermoelectrically Cooled Photo-detector

The development of scanning LADAR requires the use of a fast, light-sensitive photo-detector to detect the return signal from the target. The Discrete Amplification Photo-detector (DAPD) used in our system, is a near infrared photo-detector designed for wide bandwidth analog detection of low-level light signals with sensitivity in a single pulse down to a single photon level [39]. The detector uses internal high quality amplification process with high gain (10^5), fast response time (500 ps rise time) and ultra low excess noise factor (1.05).

In order to characterize the DAPD, a testing setup was assembled as shown in fig. 4.3. The setup consists of the 1064 nm MOPA laser operated at 1 KHz pulse repetition frequency and the DAPD. The laser beam is focused, collimated and attenuated using series of neutral density filters. The beam is guided to the detector using a dielectric coated mirror.

Lens tube with narrow band pass filter at 1064 nm is mounted on the DAPD to avoid spurious background noise. The thermoelectric cooler is connected to the DAPD to keep the detector's temperature constant at 20 C.

In order to keep the detector at a constant temperature, a thermoelectric cooler (TEC) is used (fig.4.3). TEC reads the temperature of the semiconductor using a thermistor and cools or heats up the device to compensate for temperature change. Thermistor is a type of resistor that changes its resistance value based on ambient temperature. In order to derive temperature from non-linear resistance change the Steinhart-Hart equation is used:

$$\frac{1}{T} = (C_1 \times 10^{-3}) + (C_2 \times 10^{-4})(\ln R) + (C_3 \times 10^{-7})(\ln R)^3 \tag{3.3}$$

where C_1, C_2 and C_3 are Steinhart-Hart parameters which are specific for each thermistor, R is resistance and T is absolute temperature. Steinhart-Hart parameters for our thermister are C_1=1.059, C_2= 3.149 and C_3= 1.336.

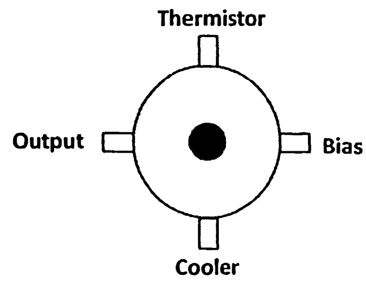

Figure 4.2. DAPD Connection Diagram

An external preamplifier ZX60-4016E-S+ is used at the detector's output to amplify the signal before observing the signal using a digital DPO 2024 scope. A low noise power supply is used to supply bias to the DAPD. The bias voltage is adjusted from 50 to 75 V and plotted versus detector's light-sensitivity as shown in fig.4.4.

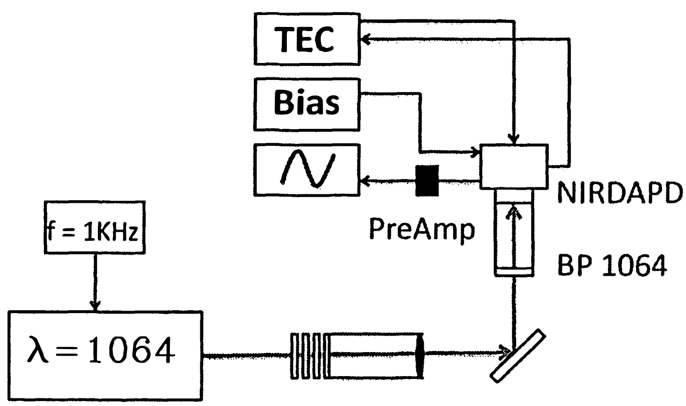

Figure 4.3. Schematic showing DAPD testing setup

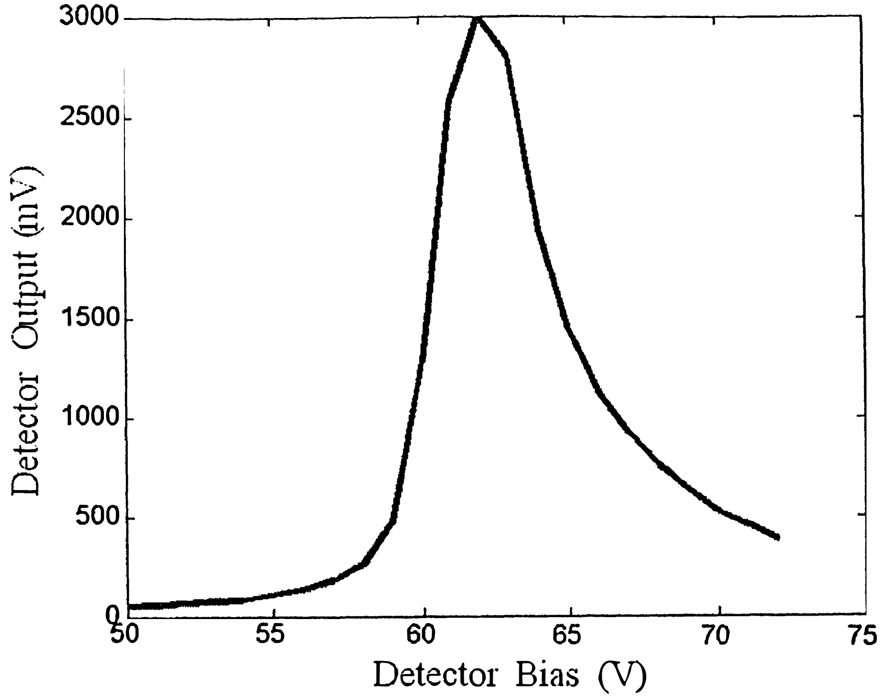

Figure 4.4. DAPD light-sensitivity measurement plotted as a function of bias voltage

Maximum DAPD response at 20^{0} C was obtained at the bias voltage of 62 V. Thus, a bias voltage close to 62 V is applied to DAPD while using it the scanning LADAR system. Fig. 4.2 shows the connection diagram for DAPD.

4.3. Constant Fraction Discriminator (CFD)

Range determination in the direct detection LADAR system is based on measurement of the time differences between start and stop detector pulses. Accurate time measurement, therefore, requires accurate triggering on start pulse and precise peak detection of the stop pulse. In certain situations, both the start and stop pulses may be unstable and may have significant amplitude jitter due to the random amplification mechanism of the avalanche photo-detector. Pulse height may also change due to laser intensity fluctuations.

A standard leading edge discriminator cannot be used in this kind of experiment because the amplitude fluctuations in the stop pulse would introduce a timing uncertainty equal to the rise time of the pulse.

A constant fraction discriminator (CFD) should be used for both start and stop pulses. The CFD triggers on a fixed constant fraction of the pulse amplitude, thus, avoiding pulse height related timing fluctuations. Constant fraction discriminator triggers on a zero cross point, which is a point at which the sum of the input pulse with a delayed and inverted input pulse crosses the zero time axis. The temporal location of the zero crossing point is independent of pulse amplitude minimizing the timing jitter caused by the pulse amplitude fluctuations. The CFD also has a built-in discriminator which rejects input pulses lower than a certain selectable threshold. This helps in reducing the noise from the preamplifiers and other electronic devices.

In our case, a CFD (Canberra Industries, Model 2126) is used. This CFD is a 200 MHz constant fraction discriminator with an independent control for threshold, walk, output pulse width and operating mode [40]. The CFD is DC coupled and has two operating modes: standard and high rate operation. In a standard mode, the CFD operates at 150 MHz with adjustable output width and dead time. In a high rate operating mode, the CFD operates at 200 MHz with fixed output and dead time. The CFD has a 50 Ω input impedance which accepts only negative pulses, up to - 5 V amplitudes. The constant fraction is set by default at 40 % of the pulse amplitude. The CFD has two independent fast negative outputs and two independent positive outputs. It can be configured to work in three operation modes: constant fraction (CF), constant fraction with slow rise time reject (SR) and leading edge (LE). The CF mode is used in our experiment.

The constant fraction with slow rise time reject mode is intended for use with detectors with variable and unstable rise times. The leading edge mode is intended for use with detectors with small amplitude and rise time variations. For LADAR time-of-flight measurement, we use the constant fraction (CF) mode because the start and stop detectors outputs have significant amplitude variations. In this mode, timing for each pulse is obtained from a comparison between 40 % fixed constant fraction ratio between the amplitude and the peak amplitude of the pulse. This method yields a time mark which is theoretically independent of the amplitude fluctuations. For better use of CFD, the pulse amplitude is delayed by using an external cable connected between two front panel 'delay' terminals. The length of the external cable is chosen to produce a time delay smaller than the rise time of the input pulse.

This leads to an output which is stabilized for both amplitude and timing jitter of that pulse (amplitude and rise time compensated timing).

For a fast rise time avalanche photo-detector such as the DAPD discussed before, a cable length induced delay of about 75 % of its rise time is necessary. The internal delay of 2126 CFD is 0.3 ns and must also be corrected using appropriate cable length. The BNC connecting cables (RG-58) produce an electronic delay of 4.8 ns/m has been used for this purpose. DAPD has a rise time of approximately 0.5 ns.

The following equation has been used to calculate the appropriate delay cable length for our photo-detector:

$$L = \frac{Delay_{total} - Delay_{internal}}{4.8} = \frac{0.375\,ns - 0.3\,ns}{4.8\,ns/m} = 1.6\,cm \tag{3.4}$$

4.4. Time to Amplitude Converter

Time to amplitude converter (TAC) is used to analyze the timing between two events in the direct detection LADAR system that occur between specific period of time. A TAC (Canberra Industries, Model 2145) has been used in our scanning LADAR system to generate a rectangular output pulse with amplitude linearly proportional to the time delay between 'start' and 'stop' input pulses. The 2145 TAC has 15 selectable time ranges from 20 ns to 1 ms. It accepts both positive and negative pulses as 'start' and 'stop' pairs. Internal gating in TAC prevents the output pulse for over range 'start' to 'stop' pulse difference, 'stop' pulses accepted prior to the 'start' pulse and 'stop' pulses accepted during the converter busy time.

The 2145 TAC produces a positive, unipolar, flat topped output which in our case is easily identified by an analog to digital converter (ADC). The output pulse is also adjustable in width from 0.5 to 2.5 μs. For each pulse width settings, the rise time of the output pulse is controlled to within 0.25 ps in order to prevent slew rate induced errors in analog to digital converter peak detection [41].

A fixed delay can be set between reception of 'stop' pulse and generation of TAC output. Positive outputs ('valid start/stop', 'valid conversion') are source matched with 50 Ω impedance, preventing ringing and pulse reflections on unterminated cables which can cause spurious effects such as multiple pulse counts. The output impedance of the TAC is jumper selectable between 10 and 93 Ω. For our current LADAR setup, user selectable 93 Ω TAC output impedance is chosen to compensate for longer cables between CFD, TAC and to drive 50 Ω ADC (NI DAQ board). The higher impedance is necessary to preserve a linear operation and response of 2145 TAC, although, it slightly reduces the output voltage.

Chapter 5: LADAR System Assembly & Computer Interfacing

Fig 5.1 shows a layout of the scanning LADAR system (Scan-LADAR) that we built in the lab. To optimize the system design, during the process, we also made CAD models of the system. Figures 5.2 through 5.4 show some of the CAD sketches of the LADAR prototype. These models will be further altered in future for compact portable design and efficient operational performance of the LADAR system.

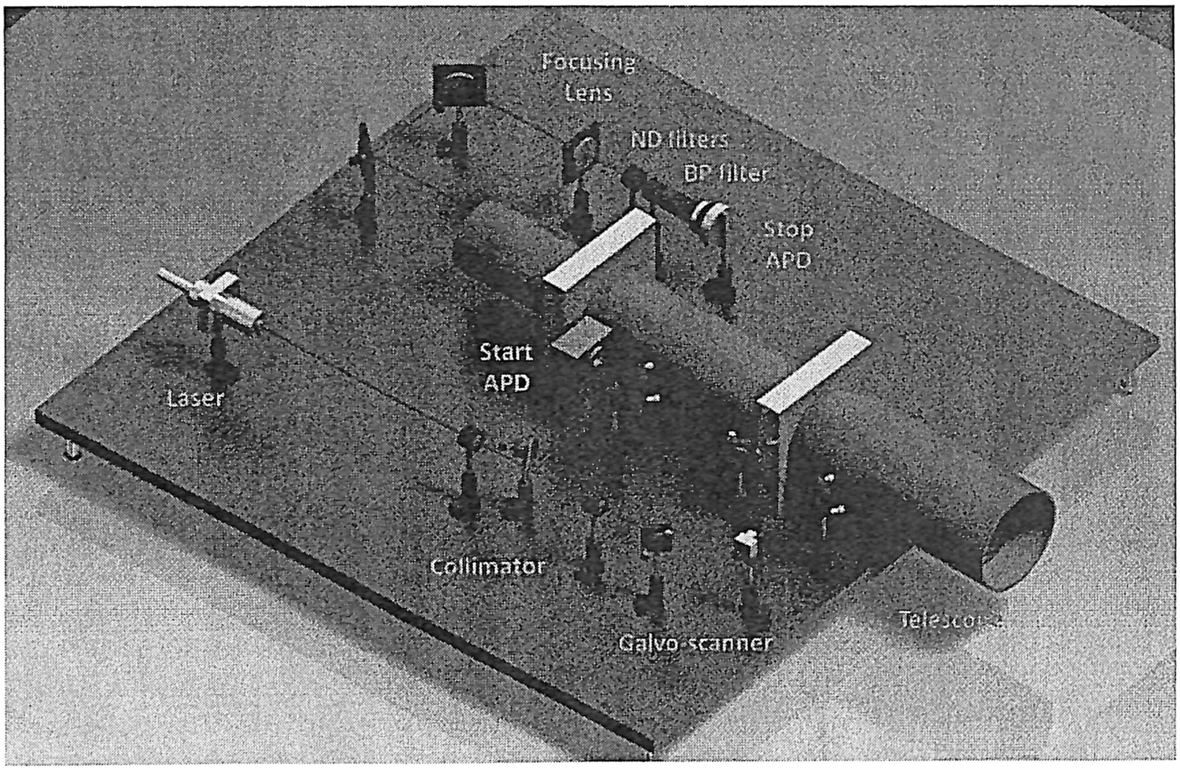

Figure 5.1. Scan-LADAR system CAD model (labeled)

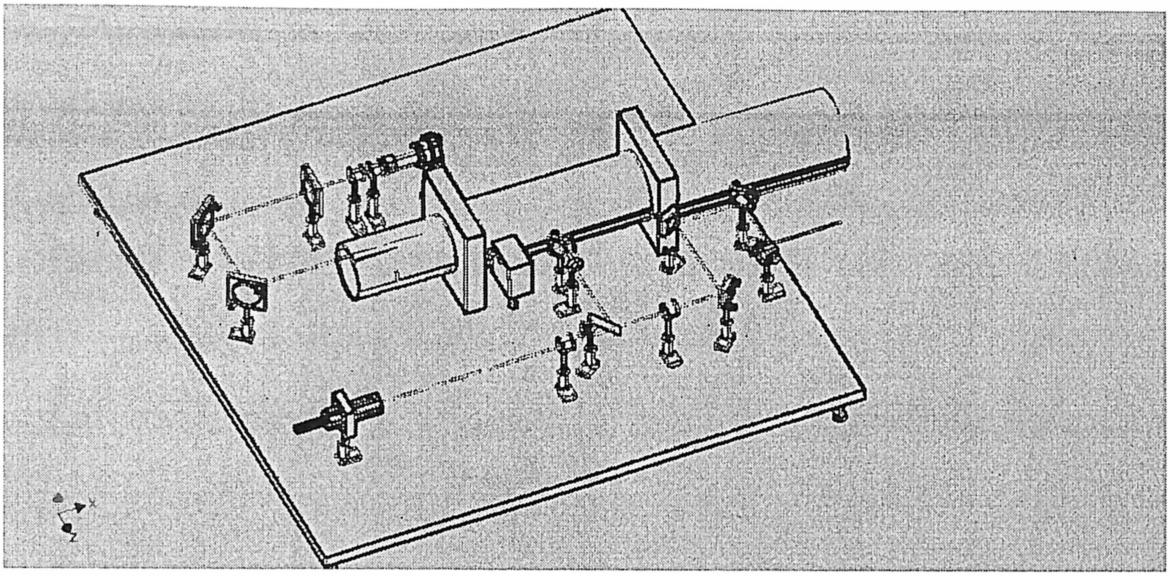

Figure 5.2. Scan-LADAR system CAD model (sketch)

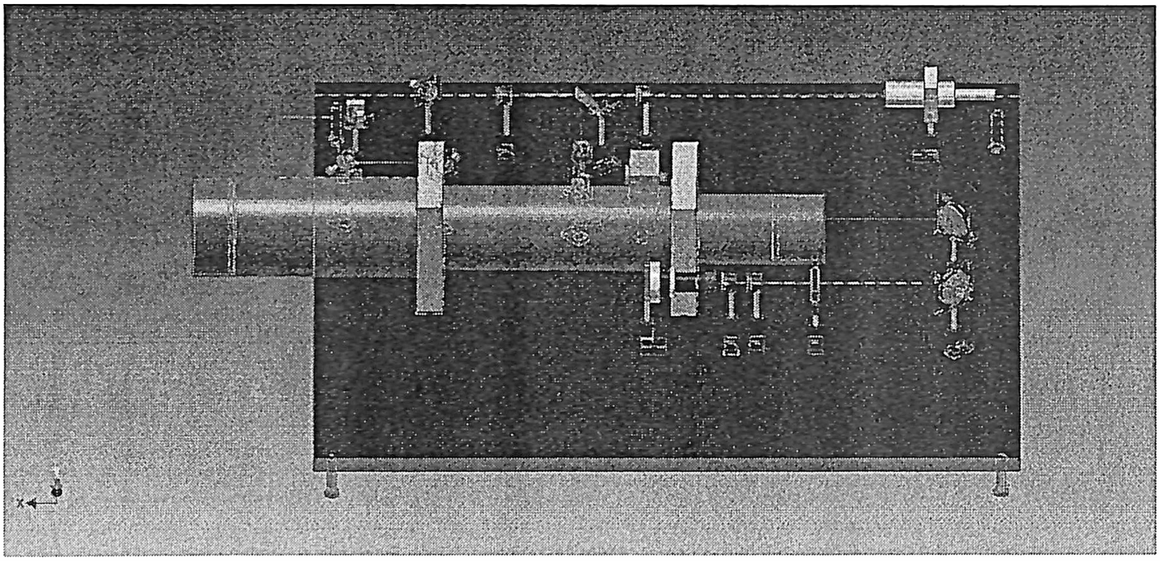

Figure 5.3. Scan-LADAR system CAD model (left side view top)

The Scan-LADAR system uses a Master Oscillator Power Amplifier (MOPA) Pulsed Fiber Laser (Multiwave Photonics MOPA-M-HP-10). This pulsed laser operates at 1064 nm, 10 ns pulses of 0.7 mJ peak energy [42]. The laser is triggered by a square wave from a function generator, and it sends laser pulses at 20 ms time intervals (50 Hz repetition rate).

The same square wave also triggers the scanning galvo-mirrors, so that the mirrors are synchronized with the laser during the scan and move synchronously by one step after each laser pulse (fig 5.4). The laser beam of 1 mm diameter at the laser-head is expanded and collimated by using two bi-convex lenses with focal lengths of 25.4 mm and 125 mm respectively, separated by a distance equal to the sum of focal lengths: 150.4 mm. The beam is expanded by a factor of 5 to reduce its divergence as it propagates to the target. A small fraction (nearly 4 %) of the laser beam is reflected by a glass slide and sent to the START Avalanche Photon Detector (APD). The rest of the beam is transmitted through the glass slide and guided onto the scanning mirrors. The scanning mirrors are used to scan the target pixel-by-pixel using a raster-scan with a 0.05 degree as minimum angular step size.

A large aperture telescope (Celesteron Omni XLT 150 mm) is utilized in the receiver arm to capture the reflected and scattered light from the target. This light is then guided through an array of mirrors and focused using 75 mm focal length lens on the STOP APD. The STOP APD used in our system is a linear mode DAPD (Discrete Amplification Photon Detector) with a near single photon sensitivity, gain in the order of 10^5, active area of 200 μm and 500 ps response time. Lens tubes, band pass filter with 1064 nm center bandwidth and a box enclosure are utilized in the setup to isolate the detector from receiving any spurious signal, thereby, reducing the probability of false alarms.

Output from the STOP APD is taken to the National Instrument high speed digitizer, which is controlled using a LabView virtual environment to capture the voltage values, corresponding to intensity of the scattered light.

A time-to-amplitude converter (TAC) is employed in the system to yield time delay (time-of-flight) between the START and the STOP pulses.

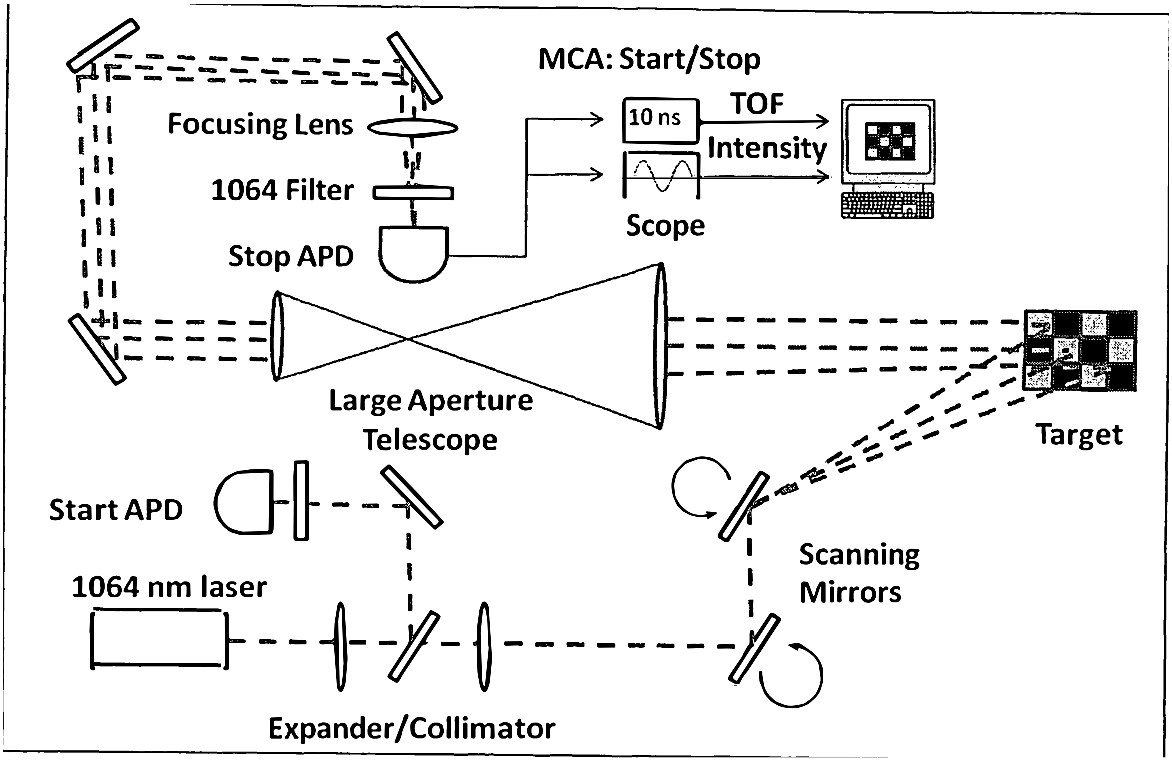

Figure 5.4. Schematic of the Scan-LADAR System

5.1. Assembly for Time-of-Flight (TOF) and Intensity Measurements

TAC is used in the system to get the TOF information. Much signal processing effort is required before the TAC could be used with analog signals. A negative START signal is sent to a fast-timing preamplifier (ORTEC model VT120C) with a sub-nanosecond rise time and a fixed gain of 20, while a positive STOP signal is sent to an inverting fast-timing preamplifier (ORTEC model VT120B) with similar sub-nanosecond rise time and a fixed gain of 200 [43]. Two constant fraction discriminators (CFDs) are used in the system to produce two NIM pulses corresponding to the START and STOP signals.

These NIM pulses are sent to the start and stop terminals of the TAC which sends its output to channel # 1 of National Instrument high speed digitizer PCI board. TAC's output is collected and voltage values are converted to distance. STOP signal is split and sent to digitizer's channel # 0 for pulse intensity measurements.

5.1a Time to Amplitude Converter (TAC) Calibration Procedure

In order to calibrate the Time to Amplitude Converter and to validate its linear voltage response to various time delays we built a setup shown in fig.5.5. We used a pulse generator (Quantum Composer) triggered by a function generator (SRS model DS345). A function generator was set to produce a square wave signal of frequency 1 kHz and a 5 V amplitude. A pulse generator was set to produce two 10 ns pulses: START and STOP with adjustable delay. A delay box (Canberra Industries model 2058) was used to introduce a constant 60 ns delay for START pulse, which was then sent to the START terminal of TAC. The STOP pulse was sent as such (without any delay) to the STOP terminal of the TAC, which was set to 200 ns time range, 2.5 μs output pulse width and 93Ω impedance.

The TAC output was connected to digital oscilloscope (Tektronix model DPO 2024). A pulse generator delay between the START and STOP signals was changed from 100 to 120 ns in increments of 1 ns and TAC output voltages were recorded. A plot of voltage verses time delay was generated and a linear relationship equation was established (fig. 5.6).

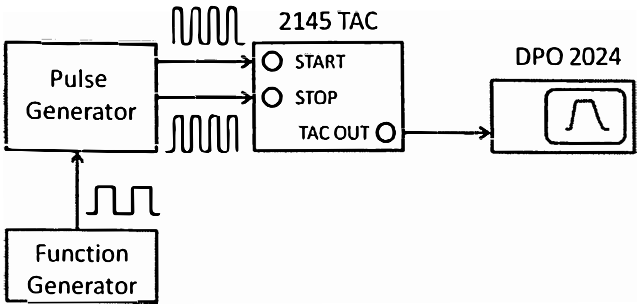

Figure 5.5. Time to Amplitude Converter (TAC) Calibration Setup

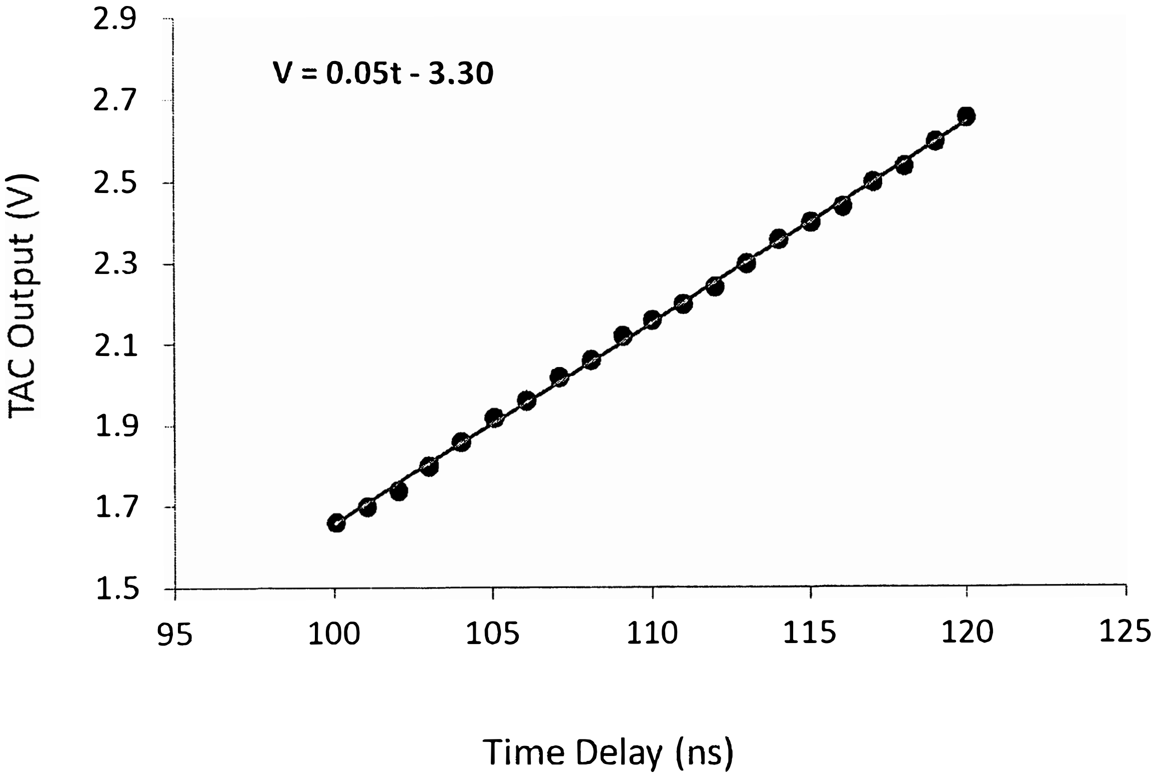

Figure 5.6. Variation of TAC Output Voltage with Time Delay

5.2. Configuration and Alignment of the LADAR Transmitter

As mentioned before, we use a 1064 nm Fiber MOPA Laser in our experimentation. This laser is randomly polarized, and operates in a pulsed mode. We use 10 ns duration pulses for our studies.

The laser beam is collimated and expanded using two lenses (ThorLabs bi-convex lenses with focal lengths 25.4 mm and 125 mm) to produce a 5 mm diameter spot size.

This step of expanding the beam is necessary to decrease the beam divergence which is crucial for large range measurements. A Keplerian beam expender design was used for this purpose. It consists of two positive focal length lenses separated by the distance which equals to the sum of their individual focal lengths. The lens closest to the light source is called the 'objective lens', the other lens is called the 'image' lens. To expand the beam, the objective lens focal length needs to be short in comparison with image lens focal length. The objective lens focuses the beam at its focal point f_1 which is also the back focal point of the imaging lens. The demagnification factor is given by the ratio of focal length of imaging and objective lenses:

$$M = \frac{f_2}{f_1} = \frac{D_2}{D_1} \tag{5.1}$$

where f_1 and f_2 are the focal lengths of objective and image lens, D_1 and D_2 are diameters of incoming and outgoing beams respectively. As already stated, we expanded the 1 mm diameter (D_1) incoming laser beam to about 5 mm (D_2) as shown below in fig.5.7.

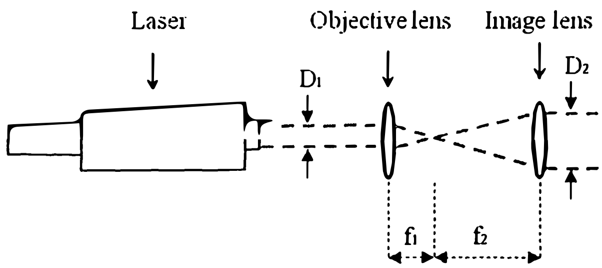

Figure 5.7. Keplerian beam expender setup

A microscope slide is inserted in the beam path close to the laser-head to send a fraction (~4%) of light to the start APD (Menlo Gmbh model 310) fig. 5.8. In order to avoid the saturation of this APD an absorptive neutral density filter (Thorlabs NE10A, ND = 1.0) is placed before it. This reduces the light intensity by a factor of 10. Rest of the transmitted beam is steered to a dual axis x-y- galvo mirror scanner (Thorlabs GVS 102).

The minimum step size of the scanning system is about 0.05 degree with full scale bandwidth of 100 Hz. We perform a raster scan of the target scene by specifying the step size and the dimensions of the scan.

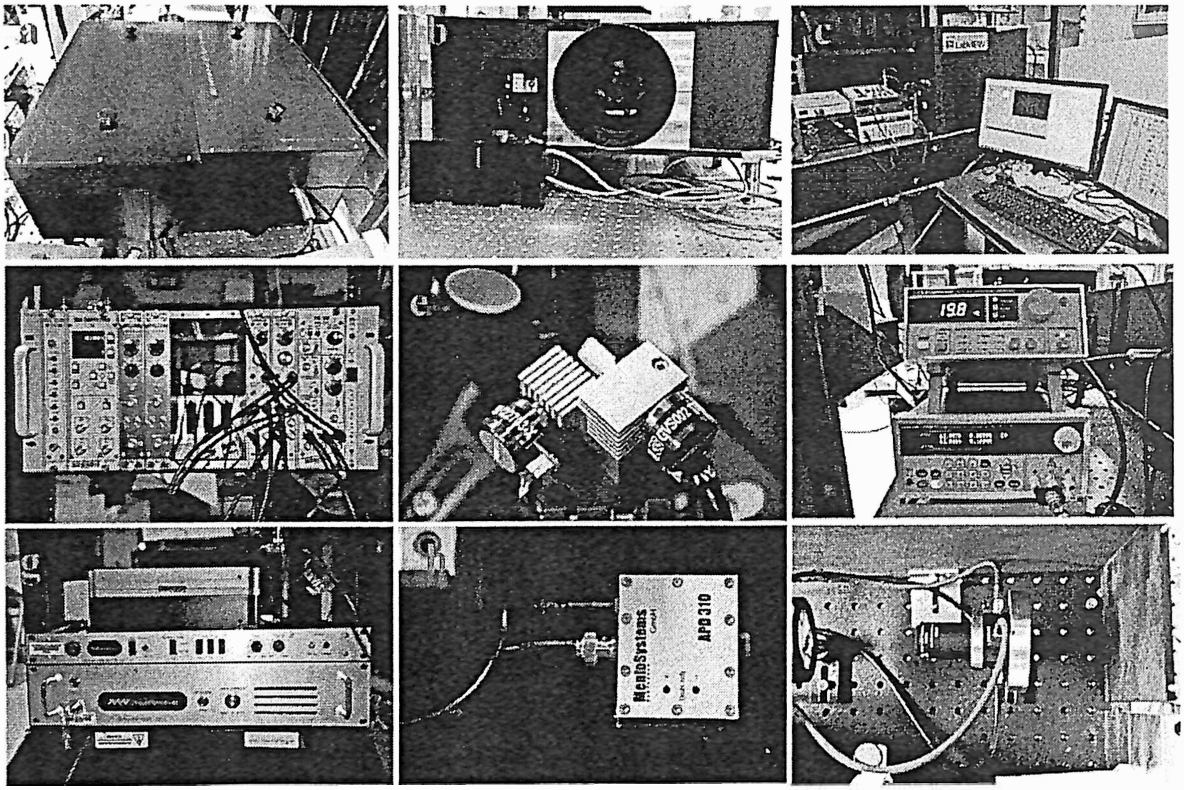

Figure 5.8. LADAR Prototype Images

a. LADAR prototype in box enclose; **b**. LADAR prototype front view; **c**. the LADAR control center and hardware; **d**.TAC, two CFDs and a delay box; **e**. scanning-galvo system; **f**. TEC controller and DC power supply; **g**. MOPA laser; **h**. 'start' APD; **i**. 'stop' APD.

5.3. Configuration and Alignment of the LADAR Receiver

We use a large aperture 150 mm telescope (Celesteron Omni XLT 150) to collect the reflected/back-scattered light signal from the target. The eyepiece of the telescope was removed to allow for a straight view of the image plane. The receiving end of the imaging system was setup as '4f' system.

After the light was focused at the focal plane of the telescope, a focusing lens was placed in such a way that the distance between the focal plane of the telescope and the lens is equal to double focal length of the focusing lens. Furthermore, the distance between the APD's aperture and the focusing lens is also equal to double focal length of the lens. A bi-convex 2 inch lens with anti-reflection coating at 1050-1064 nm and focal length of 75 mm was used as a primary focusing lens. The focal point of the telescope was detected experimentally by sending a diverged light beam from far away and observing where the beam was focused more tightly after the telescope. Another way of determining the focal point of the telescope was used to yield a more accurate result. By definition a telescope's objective lens would receive the illuminating light beam falling at a small angle to the normal and focus it at the focal point and only at that point the beam spot will not drift when the angle is changed.

The objective lens was scanned by a system of mirrors and the stationary point was detected. Based on these two measurements the focal length of the telescope's objective lens was measured to be 85 cm. The focusing lens is placed 15 cm away from the focal plane of the telescope and the APD was placed 15 cm away from the lens as shown on fig.5.9.

The beam was carefully aligned with the APD's 200 μm aperture by adjusting horizontal and vertical position of the lens and observing the intensity signal of the oscilloscope.

The point maximum intensity was set to be the right alignment of the lens. This optical configuration insures collecting of the maximum amount of light reflected from the target during the LADAR scanning. The receiving arm of LADAR system was separated from the transmitting arm using opaque dividers and was enclosed in an opaque plastic case in order to avoid unwanted background signals.

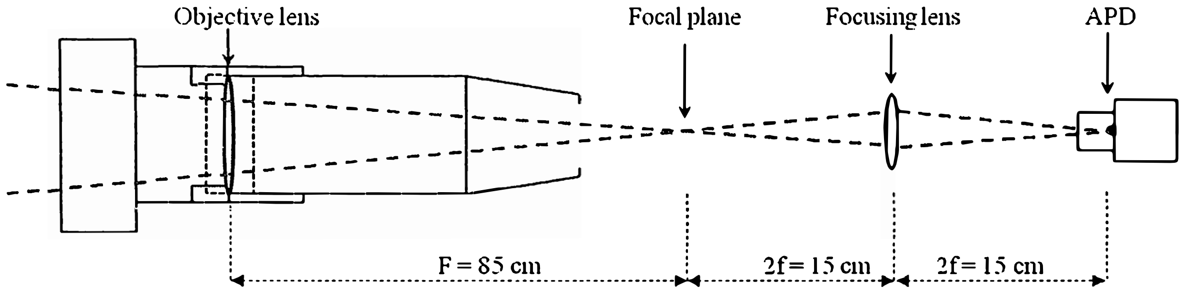

Figure 5.9. Receiving arm setup diagram *(drawn not to scale)*

The linear mode Discrete Amplification Photodetector (DAPD from Amplification Tech.) that we used in a system has already been described earlier in the section 2 in chapter 4. A temperature controller (ILX Lightwave LDT-5910B) controls the detector's thermoelectric cooler (TEC) to 10^0 C constant temperature. A programmable DC power supply (Tektronix PWS 4721) is used to control the bias voltage (62 V DC) applied to the APD. Another DC power supply (Tenma 72-8335) is used for applying a constant 12 V DC voltage to the detector's preamplifier. Lens tubes, a band pass filter (ThorLabs narrow band pass 1064 nm filter) and a box enclosure are used to reduce any spurious signal from entering the APD. For range measurements at short distances, one can expect more return signal from the target.

We have introduced measures for attenuating the signal sufficiently so as not to saturate and/or damage the APD.

5.4. Synchronized Instrument Triggering and Data Acquisition

Two data acquisition (DAQ) boards (NI USB 6251) linked to LabView virtual environment are interfaced with the computer, the receiver APD, as well as to generate trigger signals to lunch the laser pulse in sync with the galvo-scanning mirrors We also use a LabView based function generator to produce a 5 V square of frequency 10 Hz.

This square wave is split into two signals using a Bayonet Neill-Concelman (BNC) 'T' connector. One of these signals is sent to the transistor-transistor logic (TTL) trigger input of the laser, setting 10 Hz repetition rate. The second signal is sent to the servo controller of the galvo-scanner system so that the galvo mirrors move by one step with the arrival of this trigger. Thus, the laser and the galvo-scanning system are synchronized together to perform a full raster scan of a target for our measurements. We also need to trigger the receiver system to collect the data corresponding to this raster scan. This is achieved by using the start APD signal as a trigger for the digitizer, hence, eliminating the uncertainty measurement.

The output voltage values recorded by the stop APD correspond to the intensity values of light reflected from the target. We split this voltage output into two parts for intensity, and TOF measurements. As this detector's output voltage values are low, we need to amplify the signal for processing and analysis.

For intensity measurement part, we use a non-inverting fast-timing preamplifier (ORTEC VT120) which has a sub-nanosecond rise time and amplification gain of 20. Amplified stop APD's negative signal is acquired using a high speed digitizer (NI 5152).

LabView virtual environment controls the digitizer to capture the specified number of data points (~500) after each trigger which corresponds to the light return from each scanned pixel of the target. We find a peak value of the negative going signal for each data set. With data acquisition program synchronized with the laser trigger and galvo-scanner, the digitizer captures one peak value of the return light for each laser pulse & galvo-mirror position. These signal values are, saved as an array and written to file. From the intensity values thus recorded, and its corresponding positions we generate an intensity image of the target.

The signal from the start APD and the other split signal from the stop APD are used for TOF measurement. The TAC does not accept analog signals from the APD. It requires nuclear instrument module (NIM) logic with voltage of - 0.8 V as shown in fig.5.10. We use the constant fraction discriminator (CFD model 2126) to create the required NIM logic for two APD signals. The CFD however, does not accept positive going pulses. We use an inverting fast-timing preamplifier (ORTEC VT120C) for the start APD output and non-inverting fast-timing preamplifier (ORTEC VT120A) for the stop APD output to produce two negative going pulses. The TAC accepts two NIM logics from the CFDs as a start and a stop and, consequently, produces a positive output pulse with an amplitude proportional to the time delay between start and stop incidences.

The TAC output signal is acquired using the NI digitizer, peak values are detected and TOF data is saved. Combining the TOF data with corresponding position values, we generate a range image of the target.

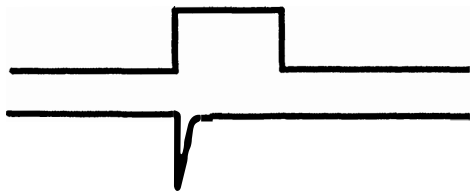

Figure 5.10. NIM logic pulse

We have described the transmitter and receiver arm configurations for the LADAR system. Next we will discuss computer interfacing of various equipment.

This is critical for the fast and efficient operation of the LADAR system and for interpreting the data obtained with it.

5.5. LabView Interfacing

The Scan-LADAR system is controlled and operated via LabView virtual environment (VI) on the computer. This program serves three main functions: i. producing the laser pulses, and raster scanning the two-axis galvo-mirror system, ii. acquiring data with the digitizer, and iii. imaging data with Matlab MathScript RT module (fig. 5.11). Our first program function is designed to control the servo-motors for the x- and y- positions of the galvo-mirrors and to create a function generator to trigger the laser. The galvanometer consists of two major components: the motor that moves the mirrors and the detector that tracks the mirrors' positions. Our dual axis glavo-scanner is based on a moving rotor-magnet and a coil, yields faster response time and higher resonant frequency compared to conventional moving coil motors. The LabView program sends two command signals to the galvo driver board each time we wish to change the position of x and y mirrors by a predetermined step size.

The driver board accepts step-signals as voltage ranging from -10 to 10 V, where 1 V corresponds to a 1 degree shift for the corresponding mirror. Maximum angular scanning range for this configuration is 10 degrees. To achieve a higher scanning range, the internal jumpers on the driver board could be set to 0.5 V per degree, effectively increasing the FOV to 12.5 degrees. The x-scan mirror is driven by a sawtooth waveform generator (fig. 5.12). The amplitude of the sawtooth corresponds to the x-range of the scan in degrees and the frequency corresponds to scanning speed. During one period of the sawtooth wave, the galvo completes one full row scan.

If we set the amplitude of the sawtooth wave to 2 V and the frequency to 1 Hz that would mean the galvo would complete one row scan of 2 degrees in 1 second per row. As mentioned above, the laser is being triggered by another waveform generator which produces a 5 V square wave signal of a specified frequency. The function generator triggering the laser is synchronized with the x-mirror generator by the system clock. These two waveforms sharing the same start trigger have constant relative frequency, and, phase relationship. We set the frequency of the square wave signal to 50 Hz so that for each row of the scan, the laser would fire 50 times in one second. The signals for x-scan mirror and laser trigger are sent through one DAQ board, making it simple to keep them synchronized. The y-scan mirror is controlled by using a voltage step function, which resembles a slow-growing sawtooth wave.

After completion of each x-scan row, the y-scan mirror moves down by one step. The scanning y- range and y- step sizes are set independently through the LabView VI.

A third function controls the NI digitizer and employs it to acquire the LADAR data. It initializes the digitizer and configures parameters such as acquisition time, sampling rate, number of samples to acquire and the trigger type.

It transfers the specified amount of data from the on-board memory of the digitizer to the Random Access Memory (RAM) of the computer. We employ both channels of the digitizer. One channel is configured to acquire intensity data, the other one collects TOF data from the TAC. The program finds a peak value of each individual waveform for intensity data '*on the fly*' and stores it in the array in the sequential order. Simultaneously, it finds the peak value of each individual waveform for TOF data '*on the fly*' and stores it as another array, in similar sequential order.

Intensity, TOF data, and peak values are stored in RAM until the data acquisition and reception is completed. Next, the peak values are saved into two separate spreadsheet files, one for intensity and one for TOF. Finally, the program plots the obtained data in the form of an image. We use a Matlab MathScript RT Module to use the Mallab features in the LabView code, making it possible to automatically generate both intensity as well as TOF images. The photograph of the scan-LADAR setup in the lab is shown in fig.5.13.

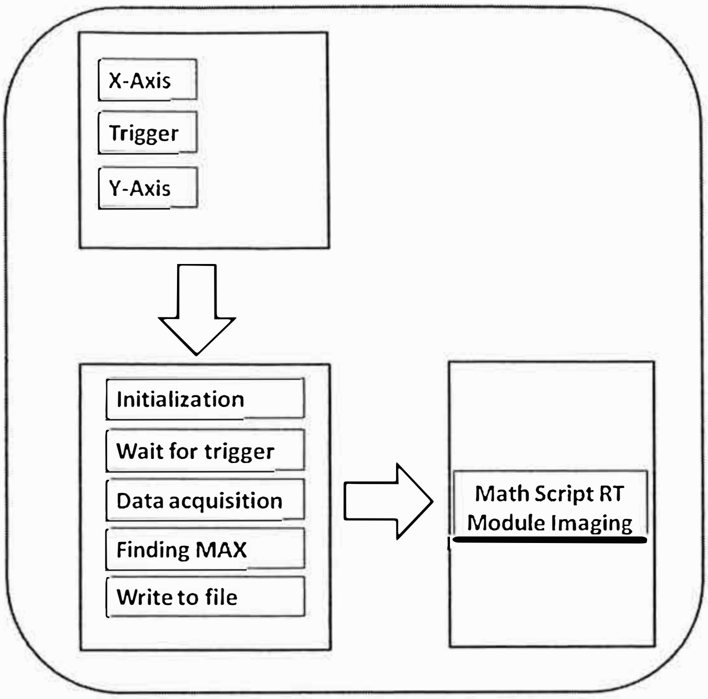

Figure 5.11 LabView program operation block diagram

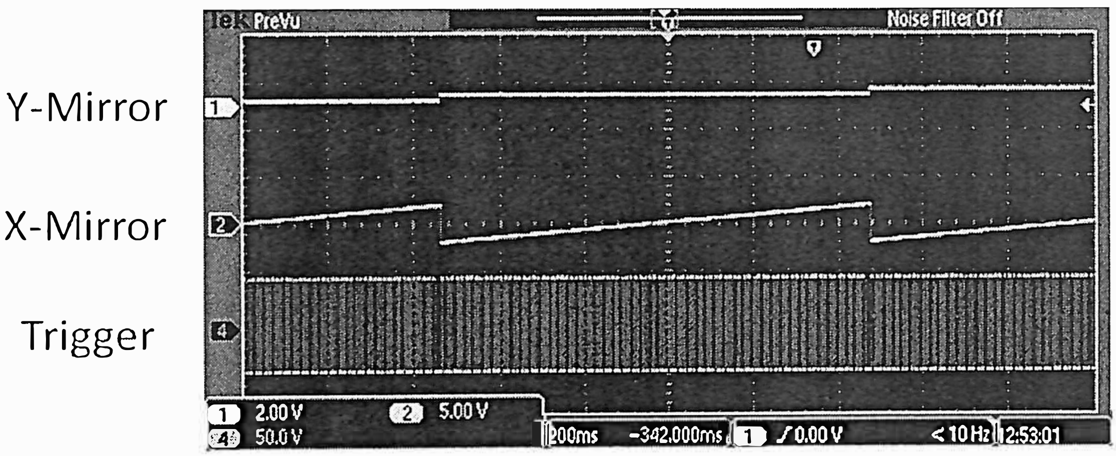

Figure 5.12 Galvo-mirrors and the laser trigger signals

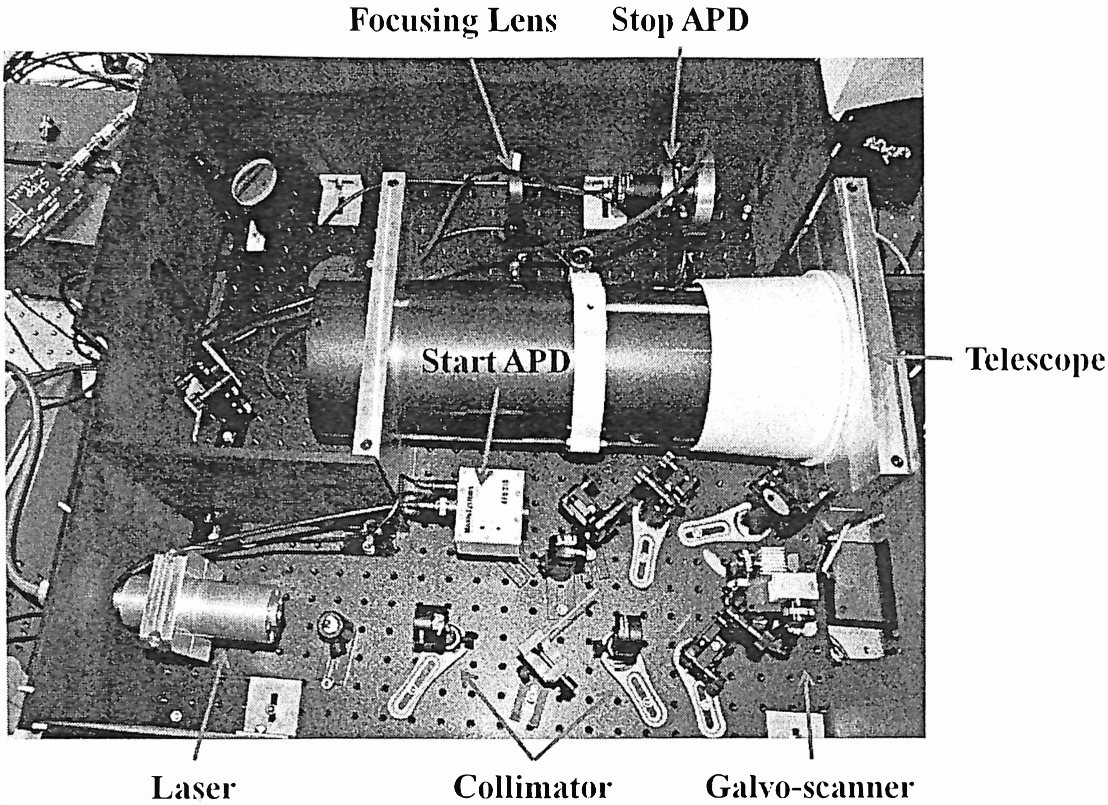

Figure 5.13. Scan-LADAR Setup in the Lab

Chapter 6: Experimental Results and Challenges

First successful image acquisition using the scanning LADAR system happened after we fixed the data acquisition issue related to the trigger. At first, we triggered the digitizer using the same square wave signal that drives the laser. This approach, even though it looks trivial, did not yield a positive result in terms of intensity data capture. The problem was that the digitizer was triggered a few microseconds before the laser started generating pulses, due to the uncertainty associated with the start of the lasing process.

As a result the laser and the digitizer were not fully synchronized, leading to missed pulse captures from the stop APD and causing discrepancies in the intensity image. After the problem was identified, we considered triggering the digitizer on the rising edge of the start APD signal, thus, avoiding the timing uncertainty due to laser pulse generation. We scanned with letter 'L' of size $(5 \times 2)\ cm^2$ and letter 'U' of size $(5 \times 3)\ cm^2$ that are cut as holes in a piece of black cardboard and located about 120 cm away from the LADAR telescope. The frequency of the galvo-mirrors was set to 10 Hz. At this speed, the scanning of a (50×60) pixels image of the object and data acquisition takes near 300 seconds (or 5 mins).

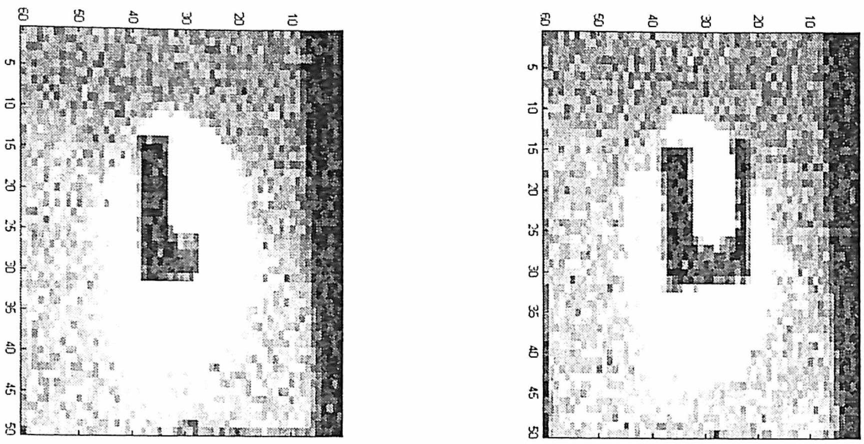

Figure 6.1. Intensity images of 'L' and 'U' shaped holes cut out of a piece of cardboard

At such a short working distance, reflection from the black, glossy surface of the cardboard seems to be high to register high gray values in the intensity image. The hole does not reflect light and therefore we can see 'L' and 'U' shaped dark regions on the image as seen on fig.6.1. Since we are using an extremely light-sensitive APD and the target is placed close to the telescope's aperture, we see a bright halo due to strong reflection in the image. This is the region where the light reflects from the target and goes directly into the center of the telescope's objective lens, also easily causing detector saturation. In order to resolve this issue, we did a series of experiments by increasing the effective attenuation of light on the detector using a stack of neutral density (ND) filters. In this case, we created a cross-shaped target by attaching two pieces of black electrical tape on a highly reflective white piece of paper.

We gradually increased the attenuation to reduce the APD saturation. Fig.6.2 shows the image collected by using a galvo-mirror scanning frequency at 10 Hz and increasing ND 0 to ND 14 as labeled in the figure (fig.6.2.). We also calibrated the ND filters at our operating for 1064 nm wavelength.

The ND 14 filter which was supposed to yield 10^{14} intensity reduction, only provided 10^{10} attenuation.

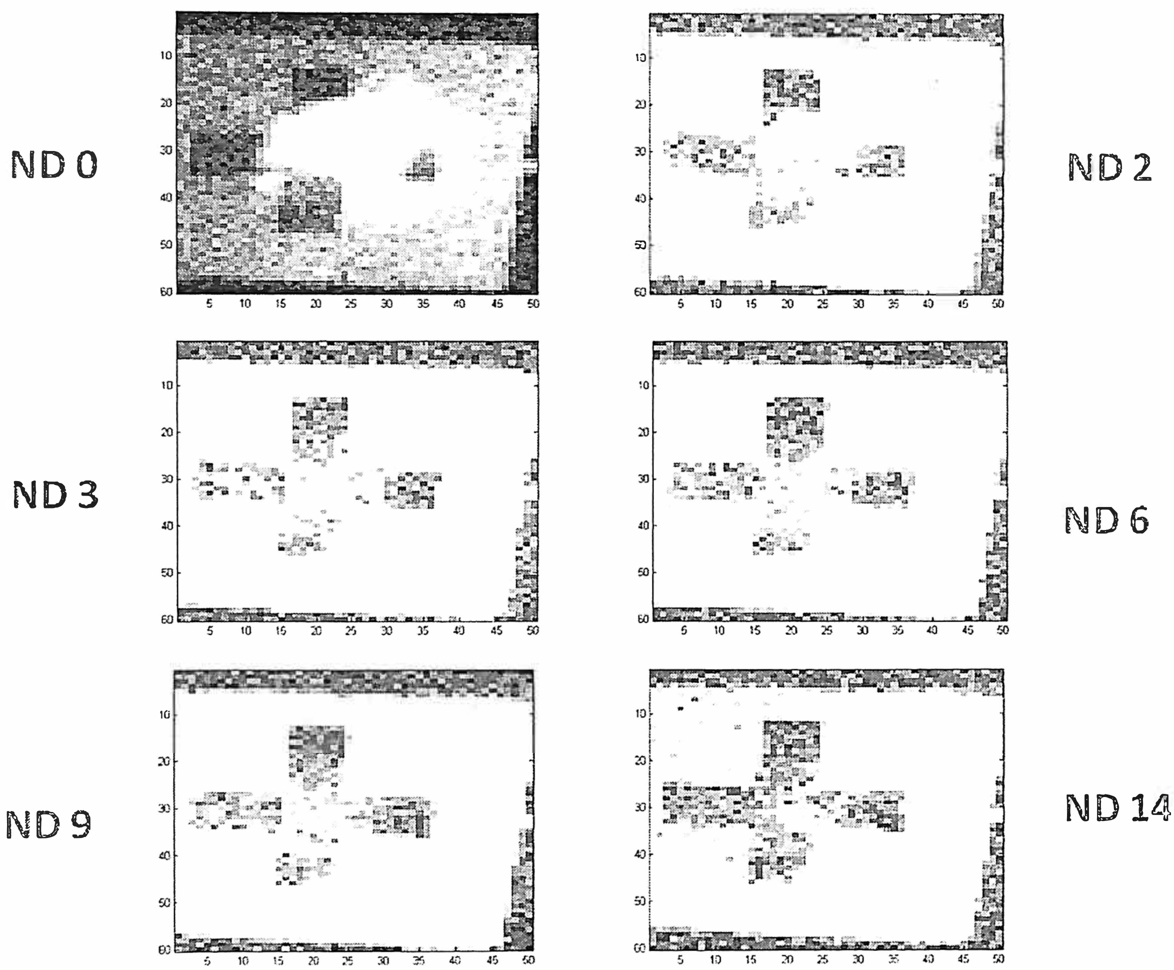

Figure 6.2. Intensity images using different ND filters showing the effect of APD saturation

6.1. Interfacing and Synchronization

After the trigger issue was resolved, and neutral density and optical band pass filters were installed, we obtained high quality intensity images of different targets with flat surface located 120 cm away from the telescope.

In order to shorten the scanning and data acquisition time, we tried increasing the frequency of the scan, and observed that the image is shifted and distorted during acquisition. The key to resolving this issue is that the galvo-mirrors and the laser should be triggered from one source, and remain synchronized during the whole scan. If this condition is not met, the captured images are distorted. The MOPA fiber laser currently used for the experiment, does not have a proper synchronization output that generates an electronic pulse each time the laser fires. This makes it difficult for us to do a proper synchronization with the scanning galvo-mirrors. Employing an optical trigger generated by a START detector helped to resolve this issue, but it did not adequately help us finding a solution to a more fundamental problem in LabView i.e. making two events happen simultaneously down to microsecond precision.

The software function generator was used to trigger the laser by sending a square wave output through the DAQ board analog output port. The galvo-mirror driving code consisted of two DAQ assistants, and LabView functions used for outputting signals into the DAQ board for x-mirror and y-mirror. The x-mirror control code was placed in a timed loop, the iteration timing of which controls the stepping speed of x-mirror. On the other hand, the y-mirror stepping speed was controlled with a simple logic code which incremented voltages and moved the y-mirror after a certain number of x-steps. The problem with this approach was that there was no feedback between the start of the software function generator triggering the laser and the start of the galvo-mirror driving code. However, the two sections of code were in the same virtual environment (VI) and were supposed to start simultaneously, but if one section executes faster than the other one, they will go out of synchronization leading to the shifted and distorted intensity images that we discussed earlier.

This kind of basic synchronization is not good enough for our demanding high-precision timing application. Ideally, we need to start the software function generator and galvo-mirror driving code simultaneously, but also their execution speeds need to be matched. In other words, if one section of the code is running slower, the other section needs to postpone the execution and wait for the first section to complete.

When the scanning frequency is set low (< 20 Hz), the simultaneous start-only synchronization is sufficient enough for the software function generator and galvo-mirrors driving code to stay synchronized. However, with the increase of galvo-mirror scanning frequency, the synchronization breaks, causing the laser to generate pulses that are not in synchronization with galvo-mirrors which creates distorted images. The most obvious solution to this problem was to introduce a fixed delay into the galvo-mirror controlling time-loop. The right amount of delay would allow the function generator and the galvo-scanner codes to catch up and keep synchronization until the scan can be completed. We introduced delays anywhere between 1 to 10 ms. Unfortunately, simply delaying one of the code sections did not prove to be sufficient for synchronization. As we can see in fig.6.3, for 10, 15 and 20 Hz the laser and the galvo-scanner are synchronized, but at frequencies higher than 20 Hz, synchronization is lost and the intensity images get distorted. By solving the trigger issue and a simple optimization of the general code, an increase in maximum scanning speed from 10 Hz to 20 Hz was achieved.

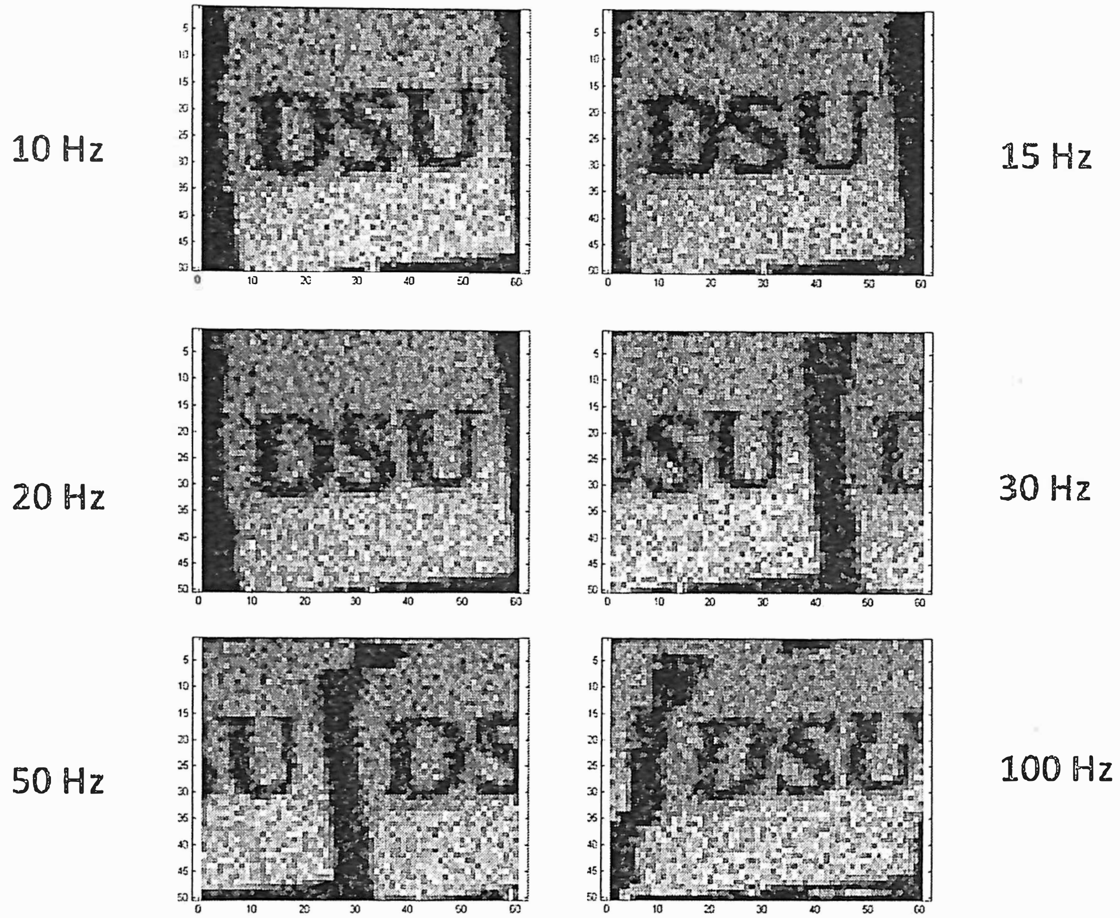

Figure 6.3. Improvement in galvo-mirror scanning speed after adding a time delay 1 ms to the galvo-scanner time loop

Another problem encountered in data acquisition was due to the use of multiple DAQ assistants for each DAQ board which significantly slowed down the entire code. We needed to use one DAQ assistant for sending the square wave trigger for the laser to DAQ board 1 and another DAQ assistant to send x- and y- controlling signals to DAQ board 2. We successfully found a way to send two signals using one DAQ assistant to a single DAQ board. That, however, created more complications since it turned out that only signals of the same type can be sent to a DAQ board using a single DAQ assistant.

That is not the case for our setup, since we needed to output two different data types such as a waveform data and a numeric data into one board. In order to overcome these limitations imposed by the predesigned functions (i.e. DAQ assistant), we used NI-DAQmx Application Programming Interface (API) for laser triggering and galvo-mirror driving. Its polymorphic VIs accept multiple data types for same set of functions which would solve one of the problems we faced while using predesigned LabView functions. This API is developed specifically for configuring data acquisition tasks. Synchronization between different devices and functions can be done more efficiently since the clock signals are automatically routed between different functions and devices. In order to implement the DAQmx API for our application, the code needed to be rewritten to change the nested timed loop structure to the state machine architecture. The state machine consists of a while loop with a nested case structure as shown below in fig.6.4.

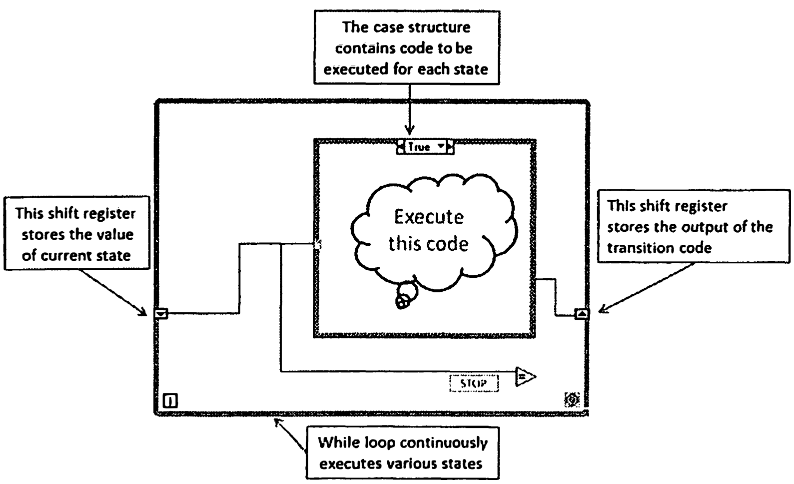

Figure 6.4. State Machine Architecture

The purpose of a while loop is to execute different states of a case structure until the 'stop' condition is met. In our case, the state machine is used to execute x-mirror scan and y-mirror shift sequentially, thus, triggering the laser continuously while the x-mirror does the scan. The software function generator was also rewritten using the DAQmx API. It was set to generate a square wave signal of fixed 5 V amplitude necessary to trigger the laser and with an adjustable frequency. The x-mirror driving code was substituted by another software function generator which produced a slow rising sawtooth wave. During one period of the sawtooth wave, the x-mirror completes one full row scan and the laser generates pulses with a frequency equal to 50 Hz. In order for the synchronization to be precise, we created a virtual channel with a common sample clock that takes care of all the essential timings in our system.

The laser and galvo-mirror driving function generators were generating the signals independently and at the arbitrary time intervals. In order to synchronize them, a common sample clock was used to feed two signals simultaneously in the virtual channel function that outputs them into the DAQ board exactly at the same time. Moreover, due to the use of common sample clock and the state machine architecture, the signals were fully synchronized, meaning that the phase difference between the two was always kept constant, as specified. The end result of this effort is, that, the laser and the galvo driving function would see two signals exactly at the same time with a constant execution speed.

The new version of the code consisted of the two independent sections. One was designed to trigger the laser and to move the galvo-mirrors synchronously. The other one was designed to control the operation of high-speed digitizer (NI 5152), capture the data, find maxima, write a data into a file, and then plot the data using Matlab graphics window for displaying intensity and range images acquired using the scanning LADAR system. At first, we tried to find an internal way of synchronization between the galvo scanning mirrors and the data capture. Later, we found a much more straightforward and simple way of synchronizing the digitizer with a galvo scanning mirrors without use of an external sample clock. This is done as follows. If we use the edge of an optical trigger after the start APD and set the threshold of the digitizer's trigger level high enough so that it cannot be triggered by noise, the only event that can start the data acquisition is the arrival of the return light received by the stop detector. Therefore, the digitizer will wait for the laser to pulse until it resumes capturing the data by triggering the data acquisition board.

Another parameter that needs to be taken into account for system speed is the data acquisition time. The digitizer's data acquisition is controlled by the 'for' loop inside the LabView code. The 'for' loop, as opposed to the 'while' loop, executes only a specified number of times N. In our case, the number of iterations N of a data acquisition loop is matched with the number of pixels in the scan, since for acquisition of each pixel of an image the digitizer needs to capture a string of data and register the maximum value as the intensity of the return pulse from the target. If the execution speed of a data acquisition loop is slow, then all of the return pulses cannot be captured. For example, if the execution speed of the loop is 20 ms, then the scan frequency cannot exceed 50 Hz, otherwise some of the data will be lost during the data acquisition process. In order to make the execution speed of the loop faster, we further optimized our code by taking the digitizer initialization and parameter setup functions outside of the loop.

We modified the code such a way that it captures the data, finds the maximum value, and registers it in the Random Access Memory (RAM) until the scan is completed. It then writes the data into a file and processes it for reconstructing the images. All these efforts yielded a system speed up by nearly a factor of 2, reducing the execution time from 20 ms to 10 ms. A further optimization can be made to reduce the overall loop timing in order to improve the system speed in future. We have collected a series of intensity images after improving the loop iteration performance using the techniques discussed above.

6.2. Measurement of the NIR DAPD sensitivity

The purpose of this experiment is to measure the minimum detectable power for DAPD. This is important in determining the maximum ranging distance for our LADAR prototype. We used our MOPA 1064 nm fiber laser, producing 10 ns pulse at 1000 Hz repetition rate. Multiple neutral density filters and a narrow optical band pass filter (bandwidth = 10 nm) at 1064 nm were installed at the detector's aperture to create a preamplified output signal which is barely above the noise floor. In this case, we measured an average power falling on the detector to be $P_{AVG} = 157\mu W$. The ND filters were calibrated to yield an effective attenuation of 1×10^5. We calculated the minimum detectable power as:

$$P = \frac{P_{AVG}}{ND} = \frac{1.57\times10^{-6}W}{1\times10^5} = 1.57\times10^{-9}W = 1.57nW \tag{6.1}$$

The energy of a single photon at 1064 nm is given by:

$$E = \frac{hc}{\lambda} = \frac{6.626\times10^{-34} J\cdot s \times 3\times10^{8} m/s}{1064\times10^{-9} m} = 1.87\times10^{-19} J \qquad (6.2)$$

Therefore, the minimum number of photons (per second) detectable by DAPD can be calculated as:

$$n_{photons/s} = \frac{P}{E} = \frac{1.57\times10^{-9} J/s}{1.87\times10^{-19} J} = 8.39\times10^{9}\, photons/s \qquad (6.3)$$

Thus, the minimum detectable energy for NIR DAPD is equal to 1.57 nW which corresponds to 8.39×10^{9} photons/second. This for a 10 ns long pulse would yield approximately 84 photons per pulse.

6.3. Laser Scanning of the Target

Laser scanning of the target is done by using a pair of galvanometric mirrors one of which is responsible for shifting the beam in the x direction and the other one in the y direction. Fig.6.5 describes such a process. The step size for these mirrors is defined as a distance between two consecutive beam spots in the x or y direction. A minimum step size is the smallest distance by which the galvo-scanner can shift the beam. Since the step size in an actual experiment is distance dependent, the resolution of the galvo-scanner is defined by the smallest angle that the motor shaft can revolve. The resolution of GVS002 scanner used in our Scan-LADAR system is 70 µrad (or 0.004° degree). Higher scanning resolution would produce a higher pixel density for intensity and range images. The laser scan in our system is performed by using a raster scan.

The raster scan is done by shifting the laser beam from left to right one step size at a time and after the row is completed, the beam is shifted down by one step size and next row scan is continued. Using this approach, it was possible to complete a rectangular raster scan of the scene with separately specified step sizes for x and y galvo-mirrors. The maximum scanning frequency for the galvo-mirrors in this process can be set to 100 Hz.

The return signal from each spot is mapped to an individual pixel which is then used to create the intensity image as shown in fig.6.5. The maximum intensity value of each target pixel is found and stored sequentially into a numerical array. By knowing the number of times the galvo-scanner stepped from left to right and also down, the code organizes the intensity values in a matrix format with an appropriate number of rows and columns. The intensity values are normalized and plotted as an intensity image either monochrome or pseudo-color.

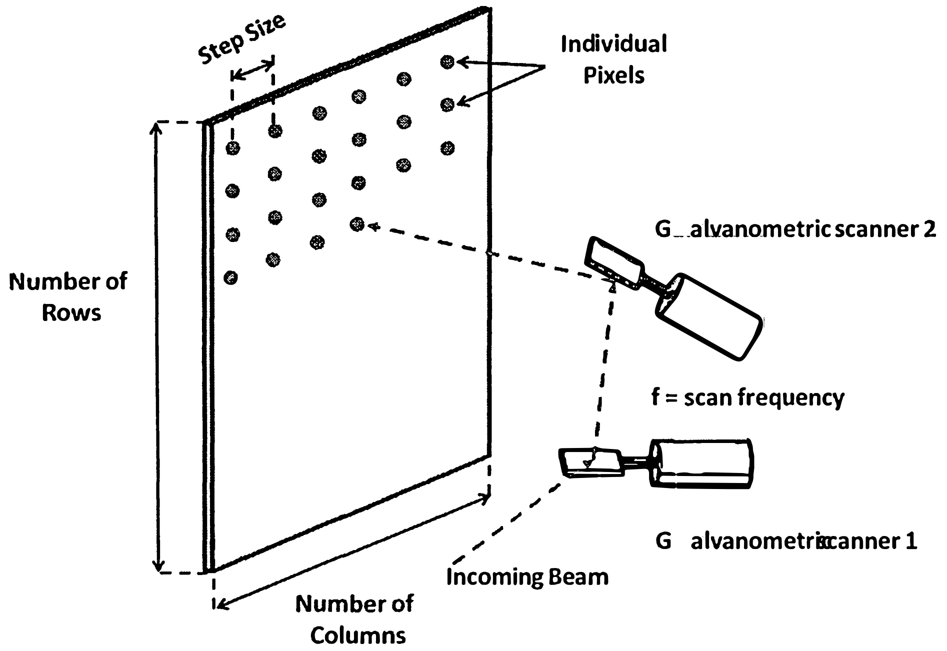

Figure 6.5. Raster scan implemented using galvanometric scanning mirrors

6.4. Data Acquisition Hardware

The performance characteristics of oscilloscopes, digitizers and other data acquisition devices need to be taken into account in intensity and range measurements in direct detection LADAR. These characteristics significantly affect the device's ability to achieve necessary signal integrity. For an oscilloscope used in LADAR's data acquisition applications, the essential characteristics are bandwidth, maximum sampling rate and record length. The bandwidth is one of the most important characteristics. It determines the fundamental ability of the device to measure a signal. Generally speaking, with an increase in signal's frequency the ability of the scope to accurately measure the signal decreases. The bandwidth specifies the maximum frequency of the signal that the oscilloscope can measure. It is defined as the frequency at which a sinusoidal input signal is attenuated to 70.7 % of its original amplitude (- 3dB point).

Without a sufficient bandwidth, the scope will not be able to resolve the pulse waveform correctly: the waveform will be distorted, edges will not be distinct, and high frequency changes will not be visible. In order to determine the oscilloscope's bandwidth required for a certain application, the '5 times rule' is applied. It will produce less than 2 % error in waveform measurement and signal display. In order to apply this rule to our Scan-LADAR system we can use the following expression:

$$\textit{Scope Rise Time} \leq \textit{Signal Rise Time} \times 0.20 \tag{6.5}$$

The bandwidth of the oscilloscope and its rise time can be related using a constant k:

$$\textit{Bandwidth} = \frac{k}{\textit{Rise Time}} \tag{6.6}$$

where k is a number between 0.35 and 0.45 depending on the scope's frequency response curve. Oscilloscopes with bandwidth less than 1 GHz typically have k of 0.35, while oscilloscopes with bandwidth of more than 1 GHz have k which is between 0.40 and 0.45. The MOPA fiber laser used in the LADAR system produces 10 ns wide pulse.

Therefore, the shortest rise time of this pulse is in the order of 1 ns. Using the above expression, the oscilloscope's bandwidth necessary to resolve a pulse with 1 ns rise time needs to be about 300 MHz – 350 MHz. The second characteristic that needs to be taken into account when selecting a hardware for LADAR data acquisition is the sampling rate. Sampling rate defines how many times per second the scope captures the signal. The higher the scope's sampling rate, the higher the resolution of the acquired signal. There is also less chance that the critical details in signal's shape will be lost.

In order to accurately reconstruct the signal's waveform on the scope's screen and avoid aliasing, the Nyquist-Shannon sampling theorem states that the sampling rate must be at least two times higher than the highest frequency component of the signal. This theorem assumes an ideal oscilloscope model with an infinite record length and continuous signal. In reality, no oscilloscope has an infinite record length and the signals are not fully continuous implying that sampling only at twice the rate of highest frequency of the signal is insufficient. Also, the accurate reconstruction of the signal not only depends on the sampling rate of the scope but also on the interpolation method used to fill spaces between the sample points. Usually, linear interpolation is used for measuring square wave type signals, while $\frac{\sin(x)}{x}$ interpolation is used for measuring the sinusoidal signals. Accurate reconstruction using linear interpolation requires sample rate to be at least 10 times the highest frequency of the signal, while $\frac{\sin(x)}{x}$ interpolation requires only 2.5 times. The 10 ns laser's pulse used in our LADAR system closely resembles a sinusoid waveform; therefore the $\frac{\sin(x)}{x}$ interpolation can be used to most accurately reconstruct it.

Another important characteristic of oscilloscope for LADAR data acquisition is its record length. It is defined as the number of points that comprise the complete waveform and determine the amount of raw data to be collected with the scope's channel. The waveform duration time is inversely proportional to the sampling rate of the scope:

$$Time = \frac{record\ length}{sample\ rate} \tag{6.7}$$

Modern oscilloscopes allow one to select any desirable record length from 100 to 1 million data points and more. When selecting a longer record length, the scopes captures a lot of data points generating a large data file. For some applications, such as direct detection LADAR system, a long record length can be inefficient and unnecessary to work with in terms of large data files. If the captured laser pulse is somewhat stable in the time domain, only 500 data points can be sufficient amount to represent the full behavior of the signal. This reduces the memory requirement and processing power requirement in order to store and further analyze the data.

6.5. Hardware Testing

In order to collect the intensity values of the reflected light from the target, the data acquisition hardware consisting of an oscilloscope, a data acquisition board or a high speed digitizer is used. We have used all three of these devices together in order to collect the data of interest. We started with NI 6251 data acquisition (DAQ) board. We wrote a LabView code which captured the data from the stop detector using 6251 DAQ board and saved it into file. However, the sampling rate of 6251 was limited to 1.25 MHz which is much below required 300 MHz to sampling rate accurately detect the peak of a 10 ns pulse. Realizing this difficulty to overcome the physical limitations of the hardware, we switched to the DPO 2124 Tektronix oscilloscope. It had a higher bandwidth of 200 MHz and a sampling rate of 2 GS/s. With these characteristics, the 2124 oscilloscope had no difficulties in acquiring the 10 ns pulse and saving it. One of the problems we encountered with DPO scope was while saving the data. By default, it only saves the data onto an external drive, which is not the way to go if we want to achieve a near real time data acquisition rate.

The universal serial bus (USB) option connecting 2124 scope to the computer and collecting the data required us to install additional software and the Tektronix drivers. The native 2124 software did not support data transfer via USB to the computer. Both LabView Signal Express (Tektronix edition) and the plain LabView environments were tested in order to synchronize DPO 2124 scope with the computer to transfer data. We came to the conclusion that for maximum performance in terms of speed and stability, the plain LabView environment needs to be used, and the use of Signal Express should be avoided due to many inherent limitations and bugs. The slow USB transfer rate did not allow the data to be transferred to the computer on time, resulting in the overflow scope's buffer memory and making it impossible to collect all data points. To overcome this issue, we used the TDS 784D oscilloscope which allowed data transfer via General Purpose Interface Bus (GPIB).

The data transfer rate of the GPIB enabled scope is faster than the USB one. After developing the code for interfacing TDS scope with LabView, installing necessary drivers and testing the data acquisition it was concluded that even though the GPIB gave some performance improvements in terms of the data transfer rate compared to the USB, it is still not sufficiently fast for our demanding high-speed application. In order to provide the necessary bandwidth and a sampling rate with an additional high data transfer rate capability, we decided to use the high-speed NI digitizer PCI 5152 (fig.6.6.) It has a bandwidth of 300 MHz, sampling rate of 2 GS/s and also the high-speed data transfer rate due to the Peripheral Component Interconnect (PCI) avoiding cables and buses which dramatically reduce the data streaming speeds. The data transfer rate for this 64 bit PCI is limited to 533 Mb/s which is more than 100 times faster than the typical USB.

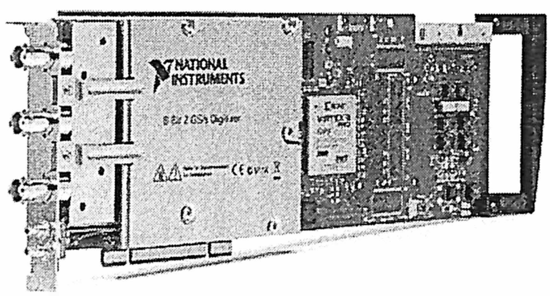

Figure 6.6. NI high speed digitizer PCI 5152 *(image courtesy National Instruments)*

We developed a LabView code that allowed interfacing PCI 5152 with a PC and acquiring the laser pulse to obtain the signal's maximum value.

6.6. Experimental Results

The purpose of the experiment was to test the operation of the scanning Laser Detection and Ranging System (LADAR) prototype developed in the laboratory. For that purpose, a simple target was constructed. It consisted of a $(7 \times 5)\ cm^2$ cardboard attached with a printed $(2 \times 2)\ cm^2$ 'DSU' letters in black ink as shown in fig.6.7. The target was located 120 cm away from the telescope's aperture. We scanned the target by employing the raster-scan method using the galvanometric mirrors. The return light was collected using the telescope. Intensity and range data were obtained using a pair of APD detectors, Time-to-Amplitude Converter (TAC) and a high-speed digitizer. The system was operated in two different modes: fast-scanning and high- resolution scanning modes.

In a fast-scanning mode, the LADAR system finished a full scan of the scene in 30 seconds producing a (50×50) pixel image. In a high resolution scanning mode, the system finished scanning the scene in 60 second producing a (90×90) pixel image. Both intensity and range images were obtained simultaneously as shown in fig 6.8.

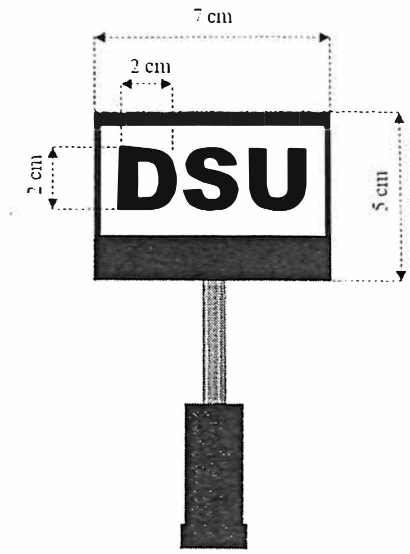

Figure 6.7. Target showing 'DSU' printed on cardboard

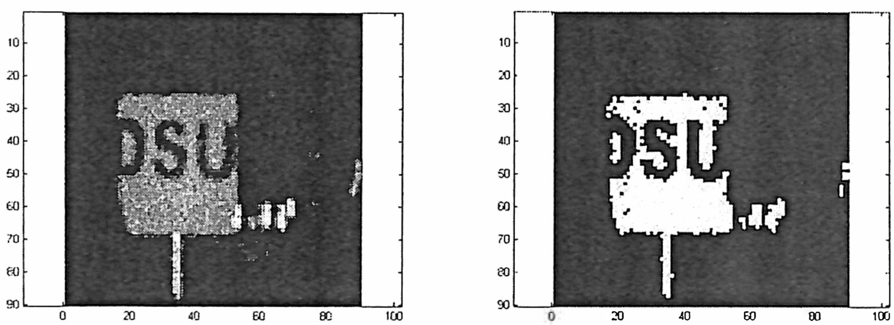

Figure 6.8. Intensity and range images obtained for the 'DSU' target taken using a high-resolution scanning mode

6.7. Spurious Ghost Images

After we fix the trigger issue, used better shielded BNC cables, increased the bias voltage on DAPD to 68 V, and reoriented the optical path on the receiving arm to make the system compact, we did a few data acquisitions as test experiments. We printed three different distinctly shaped objects on a white piece of paper in black color and used them as targets. The dimensions of these targets were as follows: elephant (7×5) cm^2, rocket

(7 × 5) cm^2 and the tree (5 × 7) cm^2. The targets were placed one by one 120 cm away from the telescope's aperture and were scanned using the LADAR system. In this case, the frequency of the scan was set to 10 Hz, since it was the maximum allowed scan frequency producing undistorted and unshifted images at that time. The intensity data was color mapped using the Matlab graphics and is shown in fig.6.9. The brighter regions correspond to a higher reflectivity surface (i.e. white paper). The darker regions correspond to a lower reflectivity surface (i.e. black picture). The contrast observed in these images is pretty high and (50 × 60) pixel image had sufficient resolution to fully distinguish the shape.

However, after a few experiments we have noticed that even if we keep the telescope's aperture closed with a black plastic lid, we still get the intensity image of the target. The black plastic lid would prevent all of the reflected light from being collected at the detector, therefore we shouldn't get any image, but it was not the case.

After a further investigation it was found that since the target was so close to the LADAR system (only 120 cm apart), the light that hits the target reflects and scatters in all directions away from the surface, also undergoes scattering from other surfaces such as the ceiling and the walls in the room goes directly into the mirrors in the receiving arm of the system.

The signal is sufficient enough to be detected by the DAPD and generate spurious ghost images. In order to avoid this issue, we had to build a black box enclosure around the LADAR system receiving arm that prevented unwanted scattered signals to interfere with the experiment. When it was done the ghost images collected with the closed telescope's aperture disappeared fig.6.10.

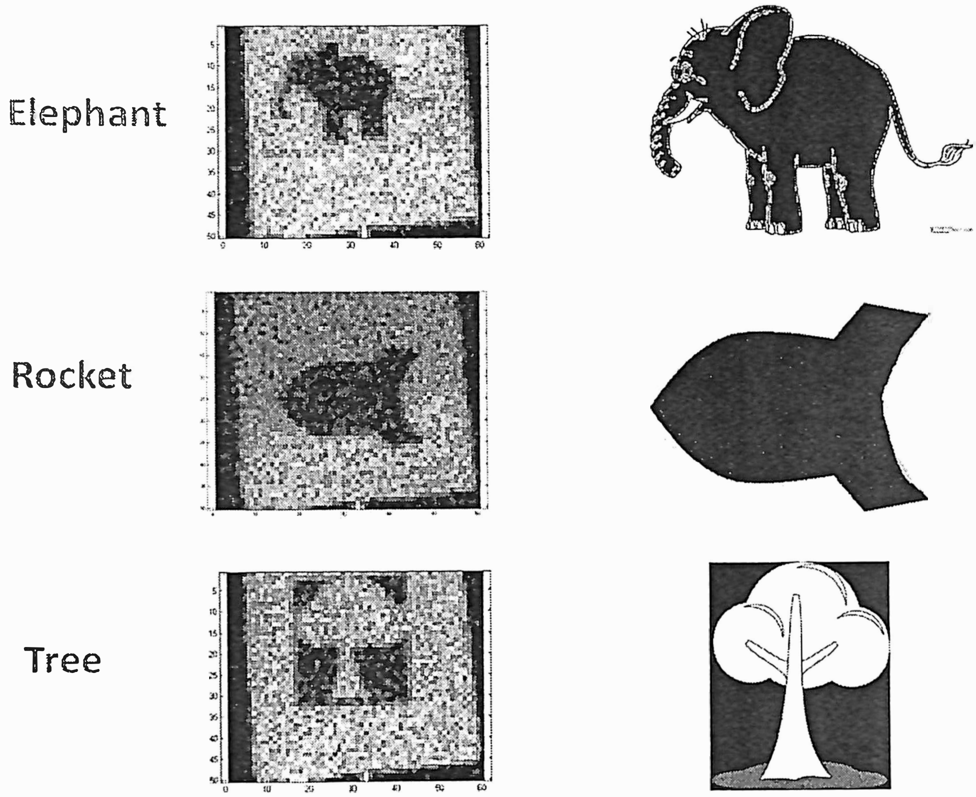

Figure 6.9. Spurious ghost images created with closed telescope's aperture

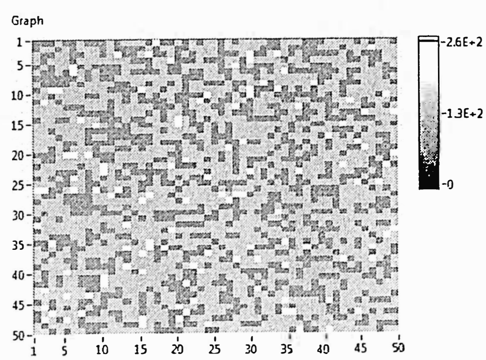

Figure 6.10. Intensity image after using the enclosure around the receiver arm

After the unwanted background signals were eliminated, and a bigger aperture (2 inch) focusing lens was installed replacing the 1 inch lens, we repeated the test intensity scans of the 'DSU' target. It had dimensions of (7×5) cm^2 and was located 120 cm away from the telescope. We did the scan at a frequency of 50 Hz and obtained the following (90×90) pixels intensity image (fig.6.11.)

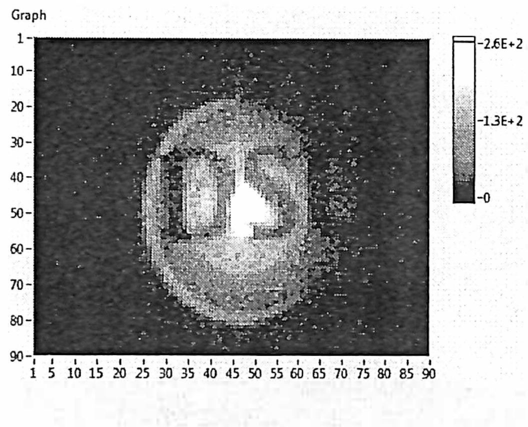

Figure 6.11. Intensity image acquired using a '4f'optical system consisting of a 2 inch lens aperture

From the intensity image obtained from the target, it became clear that the system is not properly aligned. This issue was easily resolved by using an iris and leveling the beam in horizontal plane.

The beam was guided into the center of the focusing lens and then to the center of the detector which has a size of 200 μm. The signal on the detector was maximized by viewing the beam profile on the oscilloscope and changing the positioning of the beam to hit the center of the detector. Another issue that needs to be addressed was the circular image perimeter, obscuring the target. This 'obscuration' did not allow us to see the full scene. At first, we thought that using a bigger focusing lens would resolve the issue.

We increased the diameter of the focusing lens, but the image still appeared to be cropped. The conclusion was, that due to the very narrow field-of-view (FOV) of the LADAR system, part of the target was outside the FOV causing cropping to occur.

To test this idea, we decreased the size of the 'DSU' target to $(6 \times 2)\ cm^2$, keeping the distance to the telescope's aperture fixed at 120 cm. We did a (90×90) pixel scan of the new target and obtained the following result shown in fig.6.12. The scan was completed at 50 Hz scanning frequency and took nearly 2.5 minutes to obtain the intensity image.

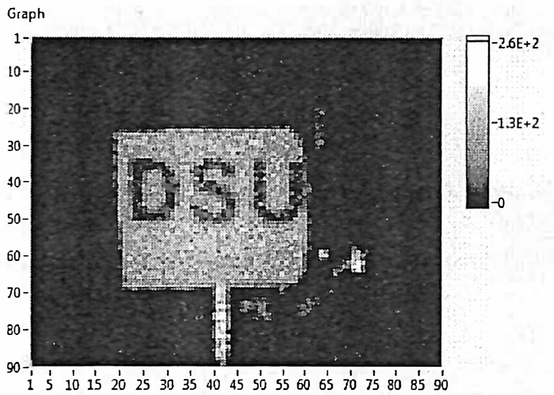

Figure 6.12. Intensity image of a smaller target that fits in the FOV of the system

The intensity image appears to be undistorted and un-shifted as shown in fig.6.13. The contrast between highly reflective white paper surface and the black color printed font appears to be fairly high. We can also decipher the reflection caused from the aluminum post at the bottom of the 'DSU' printed paper. The light dots on the background correspond to the edges of the optical table that are behind the target. After the intensity image was successfully acquired and reconstructed, we used the time-to-amplitude converter to obtain the range image of the target as shown in fig.6.13.

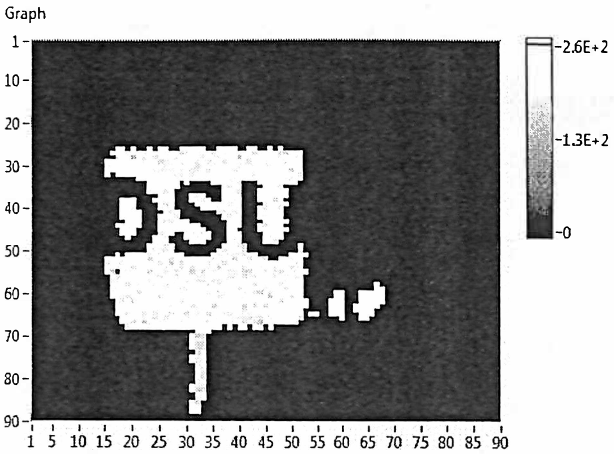

Figure 6.13. Range image of the 'DSU' target for which the intensity image is shown in fig.6.12

Contrary to the intensity image, the range image only consists of 2 colors. The dark yellow color corresponds to the voltage value produced by the TAC, which is proportional to the TOF for reflective region of the target. As we also see from the image, the table edges that are seen in the background appear lighter than the main target in the range data. This implies that they are located further away from the LADAR system than the 'DSU' target. The 'DSU' logo appears black because there is not enough light reflected back from it in order for TAC to analyze the delay.

6.8. Front panel of the LabView control interface

The front panel of the LADAR control LabView environment provides a control over the system as shown on fig.6.14. The 'start' and 'stop' signals can be observed in real-time on the oscilloscope plot in the front panel. The iteration time indicator is incorporated for testing purposes. This shows an iteration time of the data acquisition loop.

If iteration time is much greater than 10 ms under normal condition, that usually indicates a problem with alignment of the optical components or the 'start' trigger issue. There are two modes available for the scan: fast-scan and high-resolution scan as seen in fig.6.15. The fast-scan mode produces a (50×50) pixel image in about 25 seconds. The high resolution scan mode produces a (90×90) pixel image in about 90 seconds. The advantage of the fast-scan mode is its faster scanning speed, but it comes at a price of a lower image resolution.

The advantage of a high-resolution scan mode is its higher resolution image, but it comes at a price of a slower scanning speed. The x-axis galvanometric mirror speed is defined internally in the code and cannot be changed in the front panel. It is defined by the frequency of the sawtooth wave, in one period of which the galvo- mirror completes one x-row scan. In the fast-scanning mode, the frequency of the galvo driving sawtooth wave is set to 2 Hz, meaning that galvo will complete one x-row scan in 0.5 seconds. In the high resolution scanning mode, the frequency of the galvo driving sawtooth wave is set to 1 Hz, meaning that the galvo will complete one x-row scan in 1 second. The step for x scan of the galvanometric mirror is defined by the frequency of the laser. The higher the frequency at which the laser emits pulses, the smaller the step size. It is only limited by the minimum rotation angle, the mechanical parameter associated with the galvo system motor.

The laser repetition rate is set to 50 Hz for the fast-scanning mode and to 90 Hz for high-resolution scanning mode. The number of iterations defines the total number of pixels the system will capture. It is set to the value which is equal to square of the laser frequency. For the fast scanning mode it is set to 2500 and for the high resolution scanning mode it is set to 8100. The maximum range of x-axis scan is set by the amplitude of the sawtooth wave.

The y-axis galvo mirror step size is independent from x-axis and is defined separately in the front panel settings for both scanning modes. The y-axis degree range defines the maximum range of y-scan. The starting position of the scan is defined on the line orthogonal to the galvanometric scanning system when the mirrors are at the home position, meaning 45 degrees to the normal. The starting position of the scan can be altered by defining x and y offsets. The system settings for the high speed digitizer are located in the special tab in the front panel. Parameters such as trigger type, trigger level, hysteresis, sample rate, record length and so on can be changed there.

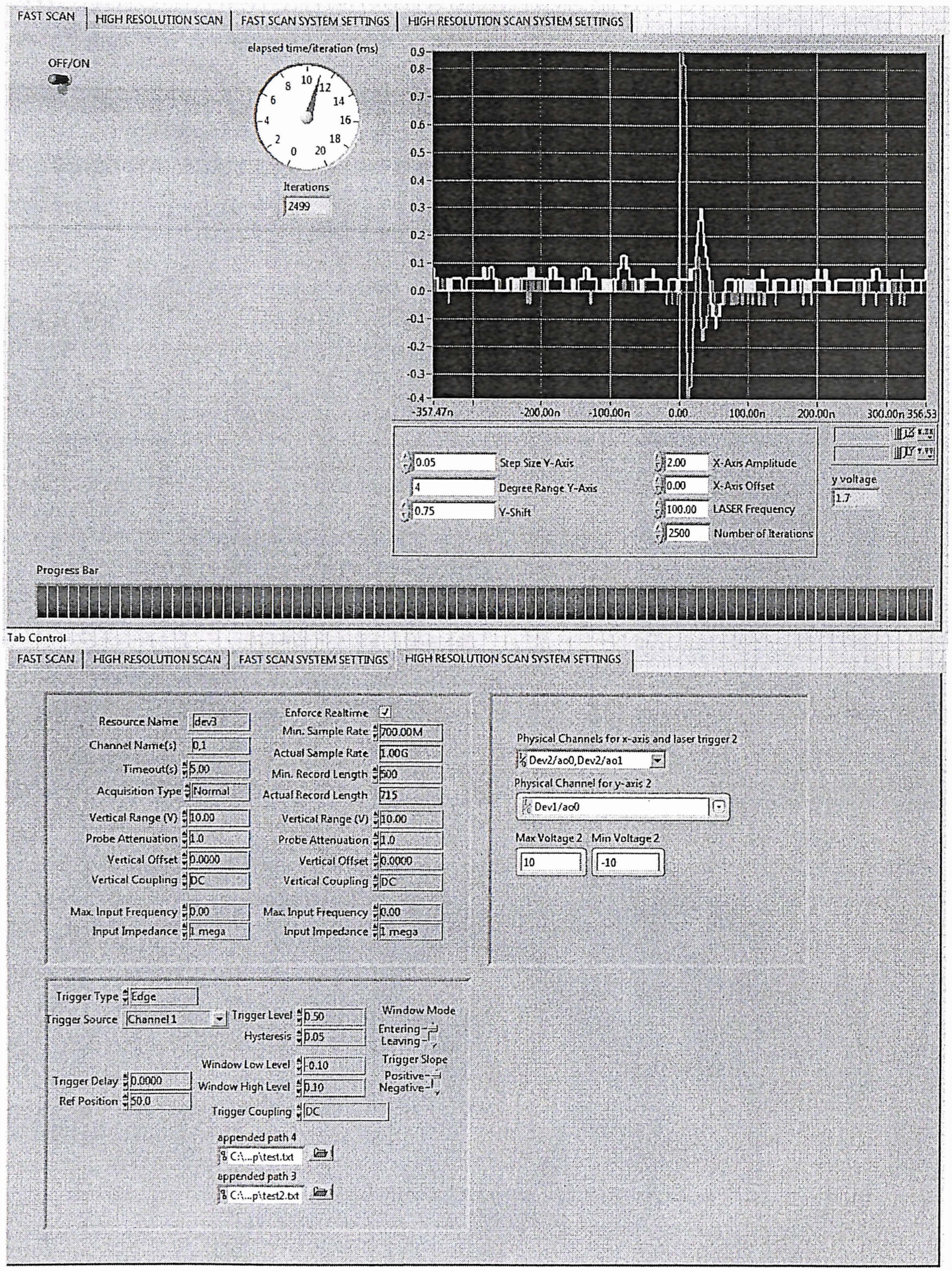

Figure 6.14. Front panel of the LabView interface that controls our scanning-LADAR system

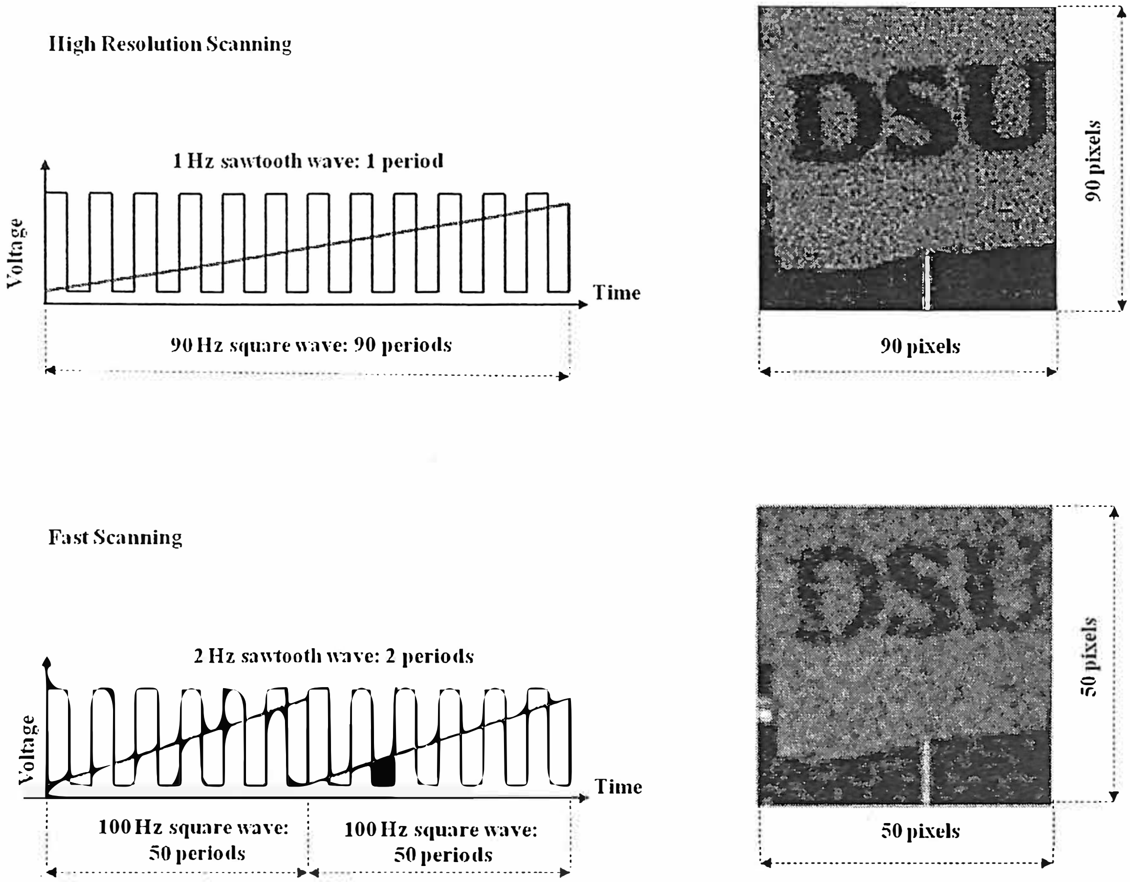

Figure 6.15. Timing diagrams for high-resolution scan and fast-scan *(drawn not to scale)*

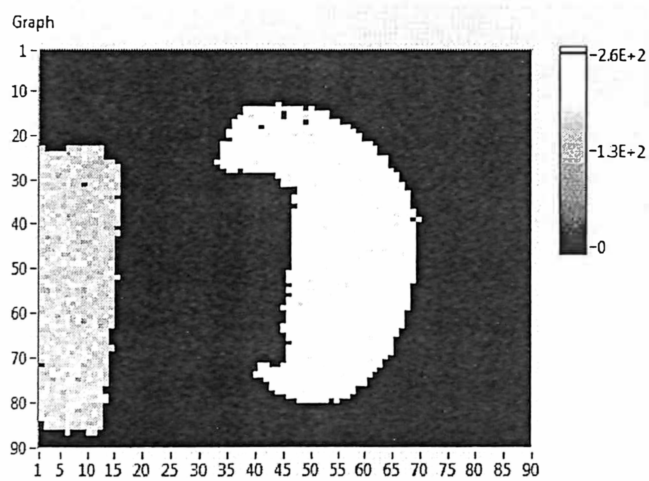

Figure 6.16. TOF Image for Two Targets

6.9. Time of Flight Measurement of Two Separated Objects

We used our LADAR system to obtain a range image of two targets separated by 30 cm distance. Each target on fig. 6.16 is color-coded to show the range information obtained from the LADAR system for a target. The object which was located closer to the system appears as dark yellow, while the object which was located further away appears as light yellow. The dark yellow color corresponds to a lower voltage value produced by TAC, which in turn translates to a shorter TOF. The light yellow color represents a higher voltage value produced by the TAC and, therefore, corresponds to a longer TOF.

Ideally, the range resolution in LADAR system is limited by the pulse duration of the laser used to illuminate the target, or more precisely, the rise time of the pulse. In case of our prototype, the laser's rise time is in the order of 1 ns, which implies that we should be able to resolve object depths to about 7.5 cm. However, due to fluctuations of TAC and CFD signals and the noise caused by the timing-jitter introduced by the electronic amplifiers used in the system, we currently cannot resolve object separation distances less than 30 cm which corresponds to about 50 mV TAC voltage output. This will be improved in future.

6.10. Conclusion

We have designed and built a direct detection Scanning LADAR system prototype based on a 1064 nm Q-switched Nd:YAG laser, fast-scanning galvanometric mirrors, a large aperture receiving telescope, and a sensitive linear mode APD with a fast rise time. The system scans a target in a pixel-by-pixel manner and collects a fraction of scattered/back-reflected light. The intensity of the light is measured by the sensitive APD and the time of flight (TOF) is measured by using a Time-to-Amplitude converter (TAC). The system control and data acquisition is achieved via LabView interface and Matlab. By acquiring the intensity and TOF data, we create the intensity and range images of a target. During the system development process, we tested and calibrated the necessary hardware components used for intensity and TOF data acquisition. At each step, we obtained the intensity and TOF images of various artificial targets to show the repeatability of the results. System performance has been improved by optimizing both the software and the optical hardware.

Our current scan-LADAR system can scan a target at a rate of 50 Hz, and produces a 50 by 50 pixels image of the same in ~ 50 seconds. The system has a depth resolution of 30 cm, which is limited by the pulse jitter and the electronic noise. The spatial resolution is limited by the divergence of the beam, which is close to 3 mrad for the laser used in the system.

Chapter 7: Future Work

In the future, we will be performing various close- and long-range field tests and incorporating new equipment in the system to improve and optimize the performance of this Scan-LADAR system. In future, we will extend some of our ideas to designing and building other LADAR systems for use in various applications. Some of the next steps planned for this work are listed below:

1. **Field test of the Scan-LADAR system.** LADAR system is typically used to scan objects at least one hundred meter away. In order to fully test the performance of our system, a long range scan test must be conducted. We will start with a building hallway-length distance scanning the targets located about 30 meters away. Targets can be placed with variable separations with respect to each other, to test the range resolving ability of the system. This experiment will also test the axial and temporal resolution of the LADAR system. Next, we will conduct long distance field tests. That would allow us to measure the sensitivity of our Scan-LADAR system in real-world conditions, since the return light would be very weak.
2. **Implement a more powerful laser source**. Currently we use a MOPA fiber laser which produces a 10 ns pulse at 1064 nm with a maximum pulse energy of 0.7 mJ. In order to achieve a greater light return from targets located at long distances, a more powerful laser is required.

We plan to use a nanosecond, diode pumped, Q-switched solid state laser (Ekspla NL 200 Series) with 4 mJ per pulse at 1064 nm.

3. **Implement faster scanning system:** In order to improve the system scanning performance and obtain a higher frame rate, the faster x-, y-scanning system need to be employed in the scan-LADAR system. We will be exploring and implementing other scanners, such as a MEMs-based scanner for achieving fast operation in LADAR imaging and ranging.

4. **Polarimetric imaging using Scan-LADAR system**. The polarimetric scan-LADAR system will have the ability to see parts of the scene not visible under intensity-only-imaging, such as objects hidden behind highly reflecting surfaces. An in-line polarimeter will be incorporated into the receiving arm of the scan-LADAR system as shown in fig.7.1 below:

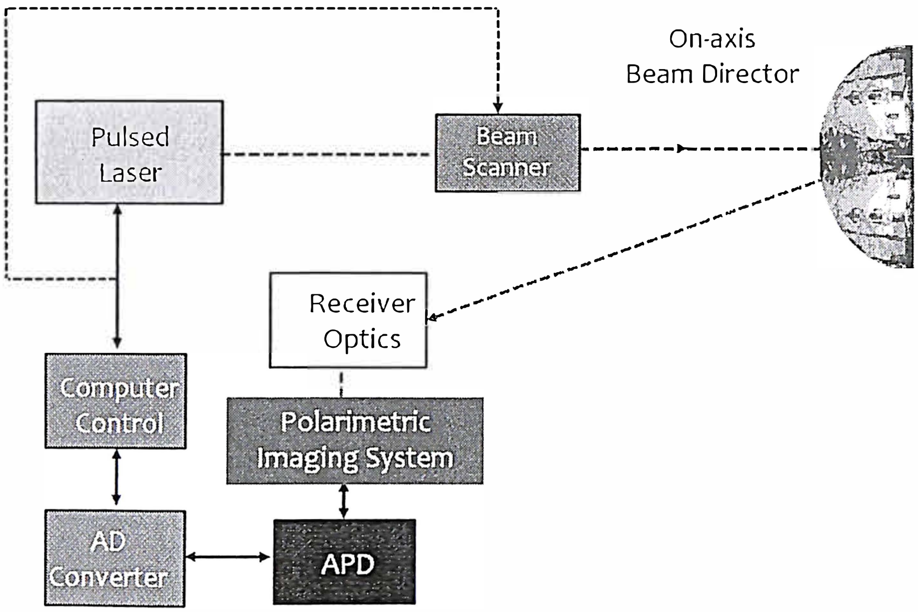

Figure 7.1. Schematic of a polarimetric Scan-LADAR System

5. **Design & build a next generation single photon counting LADAR (SPC-LADAR):** Time Correlated Single Photon Counting (TCSPC) technique offers a number of advantages over the non-photon counting LADARs.

   These advantages include improved depth resolution, thus, enhanced range resolution compared to a Scan-LADAR system. Another advantage inherent to SPC-LADAR systems is shot-noise-limited detection of single photon events, in which makes them very attractive for applications in situations where average light return from a target is extremely week (single photon approximation). The system, however, utilizes focal plane array (FPA) detectors, which are costly, and not easily available commercially. In future, we plan to build a polarimetric SPC-LADAR system for 3-D ranging and imaging in turbulent environments.

References

[1] USDA, "ARS Study Helps Farmers Make Best Use of Fertilizers". USDA Ag. Res. Service, 2010.

[2] S. Pappas, “The Light Fantastic: Using airborne LADAR in archaeological survey”, English Heritage, p. 45, 2010.

[3] J. Wilford, "*Mapping Ancient Civilization, in a Matter of Days*", New York Times, 2010.

[4] ESA, “Earth Explorers: ADM-Aeolus”, ESA.Org, European Space Agency, 2007.

[5] NOAA, "LIDAR - Light Detection and Ranging - is a remote sensing method used to examine the surface of the Earth". NOAA, 2012.

[6] NASA, “Airborne Topographic Mapper”, NASA.gov, 2007.

[7] G. Goyer, R. Watson, "The Laser and its Application to Meteorology". Bul. of the Am Met. Soc. **44**, 564, 1995.

[8] T. Wilkerson, G. Schwemmer, and B. Gentry, “LIDAR Profiling of Aerosols, Clouds, and Winds by Doppler and Non-Doppler Methods”, NASA Int. H_2O Project, 2002.

[9] Mikkelsen, Torben, Hansen, “Lidar wind speed measurements from a rotating spinner” Danish Res. Database & Danish Tech. Univ., 2010.

[10] James Ring, "The Laser in Astronomy", New Scientist June 20, 1963.

[11] NASA, “LITE: Measuring the atmosphere with laser precision”, Press release, 1994.

[12] NASA, “NASA Mars Lander Sees Falling Snow, Soil Data Suggest Liquid Past”, Press release, NASA.gov, 2008.

[13] NATO, "NATO Laser Based Stand-Off Detection of biological Agents", Online, www.nato.int, 2010.

[14] Gonglach, Matt, "How Police Laser Guns Work", Online, *www.laserjammer.net/*, 2005.

[15] M. Skolnik (Ed.), “*RADAR Handbook*”, Mc-Graw Hill, 1970.

[16] C. Bachman, "*Laser RADAR Systems and Techniques*", Artech House Inc., 1979.

[17] A. Jelalian, "*Laser RADAR Systems*", Artech House Inc., 1979.

[18] F. Ulaby, E. Michielssen, U. Ravaioli, "*Fundamentals of applied electromagnetics*", 6^{th} Ed., Prentice Hall, 2010.

[19] R. Richmond, S. Cain, "Direct-Detection LADAR Systems", SPIE Press, 2010.

[20] J. Goodman, "Statistical Optics", Wiley, 1985.

[21] G. Marshall, "Optical Scanning," Marcel Dekker, 1991.

[22] P. Besl, "Active, Optical Range Imaging Sensors," Machine Vision and Applications 1, 127, 1988.

[23] M. Albota, et al, "Three-Dimensional Imaging Laser Radars with Geiger-Mode Avalanche Photodiode Arrays," Lincoln Lab. J. **13**, Num. 351, 2002.

[24] Crowe, D.G., Norton, P.R., and Limperis, J.M., "*Detectors*", Vol. 3 (Electro-Optical Components), Ch. 4, The Infrared and Electro-Optical Systems Handbook, William D. Rogatto, Editor, SPIE Opt. Eng. Press, 1996.

[25] Anderson, C., et al., "HgCdTe APD Arrays and Readouts for 3D Imaging LADAR", Proc. SPIE AeroSense, 2002.

[26] Aull, B.F. et al., "Geiger-Mode Avalanche Photodiodes for Three-Dimensional Imaging," Lincoln Lab. J., 214, **13**, 2001.

[27] A. McCarthy, R. Collins, N. Krichel, "Long range time-of-flight scanning sensor based on high-speed time-correlated single-photon counting", Appl. Opt. **48**, 32, 2009.

[28] H. Van Trees, "*Detection, Estimation, and Modulation Theory*", Part 1, Wiley, 1968.

[29] P. Gatt, J. Thompson, and S. Henderson, "Coherent Laser Radar Range Precision for Range Resolved and Unresolved Targets, Corporation, -White Paper, Coherent Tech., 2003.

[30] W. Stone, M. Juberts, N. Dagalakis, J. Stone and J. Gorman (Eds.), "Performance Analysis of Next-Generation LADAR for Manufacturing, Construction, and Mobility", National Institute of Standards and Technology, NISTIR 7117, pp.1-4, 9-13, 20-27, 2004.

[31] M. Sweeney, G. Rynkowski, M. Ketabchi, R. Crowley, "Design Considerations for Fast Steering Mirrors (FSM's)," Axys Technologies Imagins Systems, 2002.

[32] C. Hu, and Z. Huang, "A new 3D imaging lidar based on the high-speed 2D laser scanner", National University of Defense and Technology, China, SPIE Press, 2012.

[33] Texas Instruments, "Digital Micromirror Device Delivering on Promises of "Brighter",Future for Imaging Applications," *http://www.ti.com/corp/docs/company/history/dmd.shtml*, 2004.

[34] Applied MEMS, "DuraScan Mirror Technology",

Online, *http://www.appliedmems.cc/htmlmems/index.htm*, 2004.

[35] M. Gottlieb, J. Ley, "*Electro-Optic and Acousto-Optic Scanning and Deflection*", Marcel Dekker Publisher, 1983.

[36] Spectra Switch Inc.,

www.spectraswitch.com/products/product_line/wavewalker_1x2_datasheet.htm,

2004.

[37] Beiser, L., "*Holographic Scanning*", Wiley, 1988

[38] Thorlabs Inc., "Scanning Galvo Systems: User's Guide", 2010.

[39] Amplification Technologies Inc., "Discrete Amplification Photon Detector", 2011.

[40] Canberra Inc., "Model 2126 Constant Fraction Discriminator", 2009.

[41] Canberra Inc., "Model 2145 Time to Amplitude Converter", 2009.

[42] Multiwave Inc., "MOPA-M-HP Pulsed Fiber Laser: Technical Data Sheet", 2010.

[43] Ortec Inc., "Model VT120 Fast Timing Preamplifier Operational and Service Manual", 2011.

Author Publications:

Part of the work reported in this thesis was presented in the following conferences:

1. Y. Markushin, N. Calvano, R. Tripathi, G. Pati, "Development of a Scanning Laser Detection and Ranging System for 3D Topographic Imaging ", Emerging Researchers National (ERN) Conference in STEM, Washington DC, Feb. 20-22, 2013.

2. Y. Markushin, N. Calvano, R. Tripathi, G. Pati, "Development of a Scanning Polarimetric Laser Detection and Ranging System (LADAR)", SPIE Security, Defense and Sensing, Baltimore, MD, May 5-9, 2013.

3. Y. Markushin, N. Calvano, R. Tripathi, G. Pati, "Development of Scanning LADAR System with Polarization Imaging Capability", SPIE Photonics West, San Francisco, CA, Feb. 1-6, 2014.

Curriculum Vita

Yury Markushin

423 Topaz Circle

Dover, DE 19904

Tel: (785) 317 6080

Email: ymarkushin09@students.desu.edu; ymark@thechessworld.com

Objective: Seeking employment related to optical and/or electronic devices where my expert knowledge and leadership experience will be effectively utilized.

Education:

1.Delaware State University, Dover, DE

Cumulative GPA: 3.69

M.S. *Applied Optics* Graduation date: May 2013

PhD *Optics* Expected Graduation date: May 2016

Relevant courses:

Applied Physics Experimental Research I & II, Analog Circuit Analysis, Digital Circuit Analysis, Theory of Electricity and Magnetism I & II, Material Science, Logic Circuits, Analytical Mechanics, Quantum Mechanics I & II, Electronics/Semiconductor Devices, Microprocessor Based Systems I & II, Signals and Systems Processing, Linear Optics, Solid State Electronics

2. Delaware State University, Dover, DE Cumulative GPA: 3.75

B.S. Physics/Engineering Emphasis Graduation date: May 2011

Relevant courses:

Linear Optics, Non-Linear Optics, Laser Spectroscopy, Quantum Mechanics I&II, Principles of Lasers, Advanced Electromagnetic Theory I&II.

Kansas State University, Manhattan, KS Time attended: 2005-2007

B.S. Electrical Engineering (EE)

Relevant courses:

Engineering Physics I&II, C programming

Mathematics Background: Calculus I, II and III, Elementary Differential Equations, Probability and Statistics, Grad. Mathematical Methods for Scientists

Business Background: Principles of Macroeconomics, Microeconomics, Marketing, World Politics

Computer Background:

Operating Systems:

- MS DOS, MS Windows (3.11, 95, 98, 2000, XP, Vista, 7), MS Office, Linux, Unix, MacOS

Engineering Software:

- AutoCAD, MathCAD, MATLAB, Autodesk Inventor, NI Elvis, LabView, Origin Lab, Altera, Mathematica, PCB123

Graphics Design:

- Adobe Suit, CorelDraw, Macromedia Fireworks, Flash

Web Design/Internet:

- HTML, FTP, Dreamweaver, Webpage Maker, MS-Visual Studio, SQL, PHP, ASP.NET, Blog.ENGINE, WordPress platforms, Java applications, Flash, DNS, HOSTS, IP, Joomla

Programming Languages:

- C, C++, Visual Basic, Basic, Assembler

Technical Skills:

Circuit design, optical systems design, prototype building, soldering, LAN/wireless network configuration, operating class 4 lasers, optics, and computer aided design

Research and Development:

- Graduate Research Assistant at the Photonic Imaging and Processing Laboratory (7/2011-present) Development and prototype building of the scanning polarimetric Light Detection and Ranging [LADAR] system in collaboration with NASA
- Graduate Teaching Assistant (TA) and Tutor for Physics/Math courses (9/2011-present)

- Undergraduate Research Assistant at Juxtopia Inc. Program Work/Study (1/2010-5/2011) Research and Development of an augmented reality system – design of automated lens adjustment stage based on a piezoelectric linear actuator
- Undergraduate Research Assistant (9/2009-01/2010) at DSU
  (Obtaining the size distribution of nano-particles using laser-microscopy and Laser Induced Breakdown Spectroscopy [LIBS])

- Summer Program Research Assistant (6/2008-8/2008) Design and Implementation of a Shutter Operating Circuit for Laser Induced Breakdown Spectroscopy (LIBS). Design of a printed circuit board layout for a Shutter Operating Circuit amplifier using PCB123 software
- Undergraduate Research Assistant (11/2008-12/2008) Development and Implementation of Transimpedance Amplifier for Fiber Optical Microphone
- Design and Implementation of Security System based on Altera microcontrollers (KSU 3/2007)
- Implementation of a Digital Multi Meter (DMM) (KSU 9/2005)
- Founded and currently running an internet resource www.thechessworld.com which is in top 0.3% by popularity in the U.S. among all the internet websites in the world (as of March, 2009 according to Alexa Informational Company)

Awards and Accomplishments:

- Certificate of Completion: CITI (Collaborative Institutional Training Initiative), Responsible Conduct for Research 2012
- Teaching Assistant's Effective Teaching Award 2012
- Best in Session Certificate at Graduate Research Symposium LADAR 2012
- SUMMA CUM LAUDE Honor for B.S. 2011
- Certificate of excellence in recognition of participation as Summer Research Assistant in CREOSA summer program
- The Dean's Honor Roll for Spring 2009, Spring 2010, Fall 2011
- State of Delaware Representative Bradford Bennett's recognition of Academic Excellence
- The President's Honor Roll for Fall 2009 and Fall 2010, Spring 2011
- Outstanding Academic Achievement Award Department of Physics 2010
- Certificate of Achievement for the presentation "Development and Implementation of One Dimensional Lens Adjustment System "
- Certificate of Accomplishment for CREOSA Summer Research Program 2010

Affiliated Organizations:

- IEEE (Advanced Technology for Humanity)
- Optical Society of America (OSA)
- United States Chess Federation